

**Field assessment of a concrete bridge
case study**

Lantsoght, Eva O.L.

DOI

[10.1016/B978-0-443-13470-8.00012-5](https://doi.org/10.1016/B978-0-443-13470-8.00012-5)

Publication date

2024

Document Version

Final published version

Published in

Eco-Efficient Repair and Rehabilitation of Concrete Infrastructures

Citation (APA)

Lantsoght, E. O. L. (2024). Field assessment of a concrete bridge: case study. In F. Pacheco-Torgal, R. E. Melchers, X. Shi, & A. Sáez (Eds.), *Eco-Efficient Repair and Rehabilitation of Concrete Infrastructures: A volume in Woodhead Publishing Series in Civil and Structural Engineering, Second Edition* (2 ed., pp. 139-187). Woodhead Publishing. <https://doi.org/10.1016/B978-0-443-13470-8.00012-5>

Important note

To cite this publication, please use the final published version (if applicable).
Please check the document version above.

Copyright

Other than for strictly personal use, it is not permitted to download, forward or distribute the text or part of it, without the consent of the author(s) and/or copyright holder(s), unless the work is under an open content license such as Creative Commons.

Takedown policy

Please contact us and provide details if you believe this document breaches copyrights.
We will remove access to the work immediately and investigate your claim.

Green Open Access added to TU Delft Institutional Repository

'You share, we take care!' - Taverne project

<https://www.openaccess.nl/en/you-share-we-take-care>

Otherwise as indicated in the copyright section: the publisher is the copyright holder of this work and the author uses the Dutch legislation to make this work public.

Field assessment of a concrete bridge: case study

6

Eva O.L. Lantsoght^{1,2}

¹Concrete Structures, Delft University of Technology, Delft, the Netherlands, ²Politécnico Universidad San Francisco de Quito, Quito, Ecuador

6.1 Introduction

Different methods can be used to assess concrete bridges using field data. The traditional visual inspection is one approach. Nondestructive techniques can be used to see inside the structure. These techniques can be used to locate areas of corrosion, delamination, cracking, and other structural faults (ASCE-SEI-AASHTO Ad-Hoc Group On Bridge Inspection Rating Rehabilitation And Replacement, 2009; Catbas et al., 2013; Jauregui et al., 2019; Marx et al., 2019; Thomas et al., 2012; Bertola et al., 2022). In some circumstances, cores or other material samples are taken from the bridge to determine the compressive strength of the concrete, the degree of carbonation, the amount of chlorides, and/or the grade of steel that was used. A load test can be performed to learn more about the overall structural behavior of a bridge (Schacht et al., 2016b; Alampalli et al., 2019, 2021; Lantsoght, 2019a,b; Lantsoght and Okumus, 2018a).

There are two different kinds of load tests. Diagnostic load tests make up the first category (Sanayei et al., 2016; Olaszek et al., 2014; Matta et al., 2008; Velázquez et al., 2000; Borges et al., 2021; Commander, 2019; Lantsoght et al., 2019a; Albraheemi et al., 2019; Bonifaz et al., 2018; Hernandez and Myers, 2018), in which the structural response to a known load is determined. After that, the measured structural response is contrasted with the analytically or numerically predicted response, and this comparison can be used to update the bridge's numerical model to create a model that is considered as field-validated. Finally, the load rating of the bridge can be carried out in a way that takes into account the measured behavior. Rating will require adjusting the field-validated model for rating purposes. The load levels required for diagnostic load testing are relatively low, as the primary goal is to achieve a measurable structural response (Alampalli et al., 2019, 2021). Typically, 60%–70% of the serviceability traffic load combination is used (Ministerio De Fomento and Direccion General De Carreteras, 1999). Diagnostic load tests thus can be done at a lower cost. These types of tests can be used to compare with an analytical model. By studying the differences between the analytical model and the response in the field, it is possible to identify factors that differ from the assumptions of the analytical model. Examples of such differences, which can occur individually or in combination, depending on the type of bridge, are the contribution of nonstructural

elements, unintended composite action, the effect of frozen bearings, transverse load distribution, etc. (Barker, 2001).

Proof load testing is the second category of load testing (Lantsoght et al., 2016c, 2017a,b,e, 2018b, 2019b; Liu et al., 2014; Faber et al., 2000; Lin and Nowak, 1984; Koekkoek et al., 2016; de Vries et al., 2022; Wang and Zhang, 2020; Frangopol et al., 2019; Val and Stewart, 2019; Vavruš et al., 2019; Chen, 2019; Halicka et al., 2018; Halding et al., 2018). A load representative of the factored load combination used for the assessment of the bridge is applied during a proof load test. The proof load causes the same sectional shear or moment as the factored load combination. The proof load test is successful, and it has been demonstrated experimentally that the bridge is capable of carrying the loads specified by the code if it can carry the proof load without showing any signs of distress. The bridge may still satisfy lower levels of the code's requirements if it exhibits signs of distress before it reaches the target proof load. Based on thresholds for the measured structural responses, stop criteria are followed during the test. The term "stop criteria" refers to these thresholds (Christensen et al., 2021, 2022; Zarate Garnica et al., 2021; Zarate Garnica and Lantsoght, 2019, 2020; Lantsoght et al., 2018c,d, 2019c; Paredes and Lantsoght, 2018; Rodriguez and Lantsoght, 2018; Yang et al., 2018, Halding et al., 2018): when a stop criterion is reached, further loading of the bridge is not allowed, and the test ends at the load level at which the stop criterion is reached. When there are significant uncertainties that make it challenging to determine the structural response analytically, proof load testing may be the best option. These uncertainties include the impact of material deterioration, uncertainties resulting from a lack of knowledge when structural plans are absent, and uncertainties with regard to the load path at higher load levels.

The ultimate capacity of the tested bridge cannot be determined by any type of load test. A collapse test may be considered if the bridge is decommissioned and the ultimate capacity must be determined (Lantsoght et al., 2016a,b, 2017c; Bagge et al., 2015; Nilimaa et al., 2015; Puurula et al., 2014, 2015; Ensink et al., 2018, 2019; Haritos et al., 2000).

Analytical assessment of a bridge is challenging for bridges with damage caused by alkali-silica reaction (ASR), as the effect on the capacity is not fully understood. The alkali in the cement reacts with the silica found in certain types aggregates to cause this reaction, ASR. This reaction produces a gel. This gel will expand when it comes into contact with moisture. Stresses in the concrete are a result of this expansion. Concrete will crack if these stresses are tensile stresses larger than the concrete's tensile strength. Unless the level of expansion caused by the ASR-gel is high, experimental research has shown that ASR damage has little impact on the bending moment capacity (Talley, 2009). For reinforced concrete members, the reinforcement steel partially offsets the expansion, creating a prestressing effect. This hypothesis is supported by tests of reinforced concrete members with and without ASR damage, which reveal that the prestressing effect of the ASR increases the cracking moment for the ASR-damaged specimens (Haddad et al., 2008).

Given that cracking lowers the concrete's tensile strength, the shear capacity of elements with ASR damage is up for debate (Siemes et al., 2002). According to some authors, laboratory testing for shear capacity results in higher shear capacities

(the advantageous prestressing effect is credited for this) (Ahmed et al., 1998, 1999), whereas testing of beams (den Uijl and Kaptijn, 2004) cut from slabs of ASR-affected viaducts resulted in a reduction of the shear capacity by 25% compared with Rafla's formula (Rafla, 1971). In addition, a number of load tests on viaducts affected by ASR were reported (Talley, 2009) in South Africa, Japan, France, Denmark, and the United States (Schmidt et al., 2014). These load tests demonstrated that ASR does not significantly influence the overall structural response of the tested bridges. These few studies, however, are insufficient to deem all ASR-affected viaducts structurally safe. Proof load testing allows for the analysis of specific cases. The proof load testing of the Zijlweg viaduct, which is affected by ASR, is discussed in this chapter.

6.2 Case study: the viaduct Zijlweg

6.2.1 Viaduct description

The Zijlweg viaduct crosses the A59 highway and is situated in the Zijlweg road connecting Raamsdonksveer and Waspik. Owned by the Dutch Province of Noord Brabant, the bridge was constructed in 1965. The original live loads were calculated for traffic class B, using a distributed lane load of 400 kg/m², and a design truck with two axles of 10 tons each and one axle of 20 tons. The original service life was 80 years. Fig. 6.1 contains a photo of the viaduct.

The Viaduct Zijlweg is a reinforced concrete solid slab bridge with four continuous spans and built at a 14-degree skew angle. The central spans are 14.71 m long, while the end spans are 10.32 m long. Fig. 6.2 depicts the viaduct Zijlweg's overall geometry. The thickness varies parabolically between 550 and 850 mm. The cross section measures a total of 6.6 m in width, including the carriageway's width of 4 m. Elastomeric bearing pads are used at the supports, and the spans are supported by concrete piers at the central supports and by an abutment at the end supports.

The history of the bridge is reasonably well documented. The original calculation report (Provincie Noord Brabant, 1965) is available. In 2002, repair work was done; a report on the work, along with a management and maintenance plan, is available (Rijkswaterstaat, 2002) (2008) as well as a recent inspection report (Gielen et al., 2008). Inspections are scheduled to occur every 5 years. To stop further moisture intrusion, a waterproofing layer was added to the top side of the slab during the 2002 repairs. According to the results of the 2008 inspection, the viaduct is in moderate condition. The potentially insufficient capacity of the superstructure was considered a high risk. As a result, it was noted that the viaduct does not fully satisfy the performance criteria and poses a higher risk of failing to carry out its essential functions in a safe manner.

6.2.2 Monitoring of alkali-silica reaction

In the Province of Noord Brabant, a large number of bridges over the highway A59, including the viaduct Zijlweg, showed signs of alkali-silica reaction (ASR).



Figure 6.1 Photograph of viaduct Zijlweg: (A) top view; (B) bottom view.

This damage was first detected in 1997 (Projectteam RWS/TNO Bouw, 1997). The same materials were used to construct all of these bridges in the same era. The ASR damage led to cracking in the Zijlweg viaduct. Many of the concrete cores that were removed from the viaduct had uniaxial tensile strengths of 0 MPa because they were completely intersected by cracks. Other cores still possessed some uniaxial tensile strength, but this strength was much lower than would be predicted by using expressions as a function of the compressive strength of the concrete. Since flexure-shear failure is a diagonal tension failure, concerns were raised at the time regarding the shear capacity of bridges with ASR damage due to the concrete's low uniaxial tensile strength. These slab bridges were not reinforced against shear (i.e., no stirrups were provided in the cross section), in addition to having low uniaxial tensile strength and significant cracking. Additionally, the bridges were built to withstand lower live loads and higher shear capacities than what the current governing codes require.

in the concrete, and longitudinal expansion of the deck. Additional sensors were installed on measurement locations 8–10 in the middle of 2007 after being installed on measurement locations 3–7 in 2003. Since April 1, 2003, measurements have been taken hourly. The inspection report (Gielen et al., 2008) assessed the ASR monitoring's outcomes. It was observed that the viaduct's longitudinal expansion had reached its maximum value. The monitoring system's readings can be contrasted with the official Dutch meteorological institute's readings of the surrounding air temperature. Gilze-Rijen, 14 km south of the Zijlweg viaduct, is the chosen location. The experimental report contains an extensive analysis of the data of the ASR monitoring in combination with the meteorological readings (Koekkoek et al., 2015). There is a noticeable relationship between the thickness, joint size, and moisture content in every plot and the surrounding temperature. While the joint size is inversely correlated to temperature, the average deck thickness tends to follow the ambient temperature trend (see Fig. 6.4). As the deck expands more in the longitudinal direction as a result of rising temperatures, the joint size decreases. As a result, the observed data confirm the predictions. The data also show that the ongoing moisture increase is limited and only observed at one measurement point.

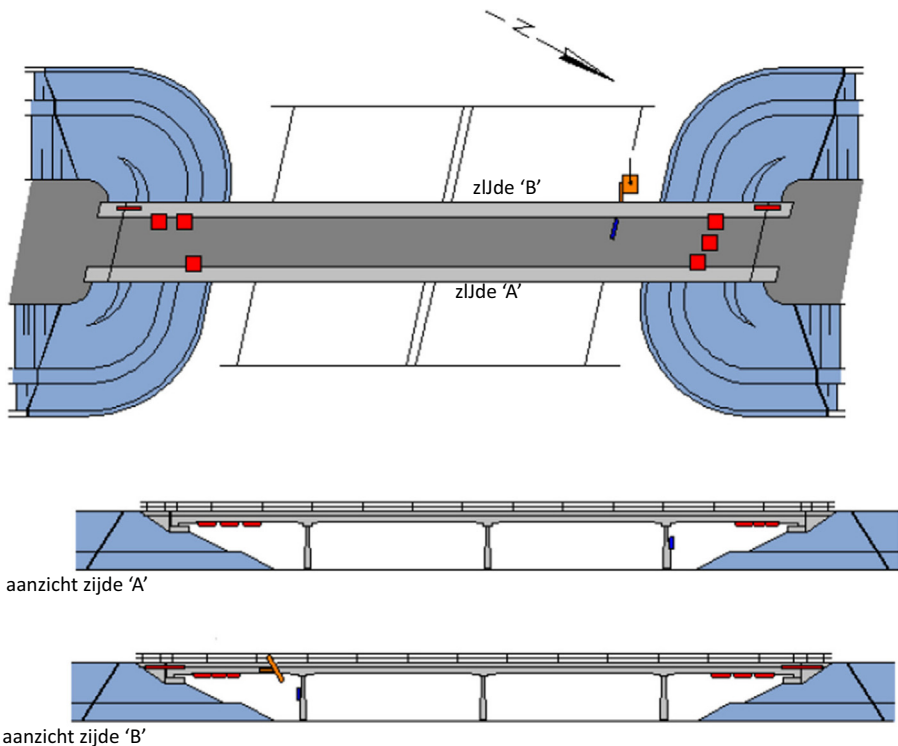


Figure 6.3 Monitoring system for ASR on viaduct Zijlweg. ASR, Alkali-silica reaction.

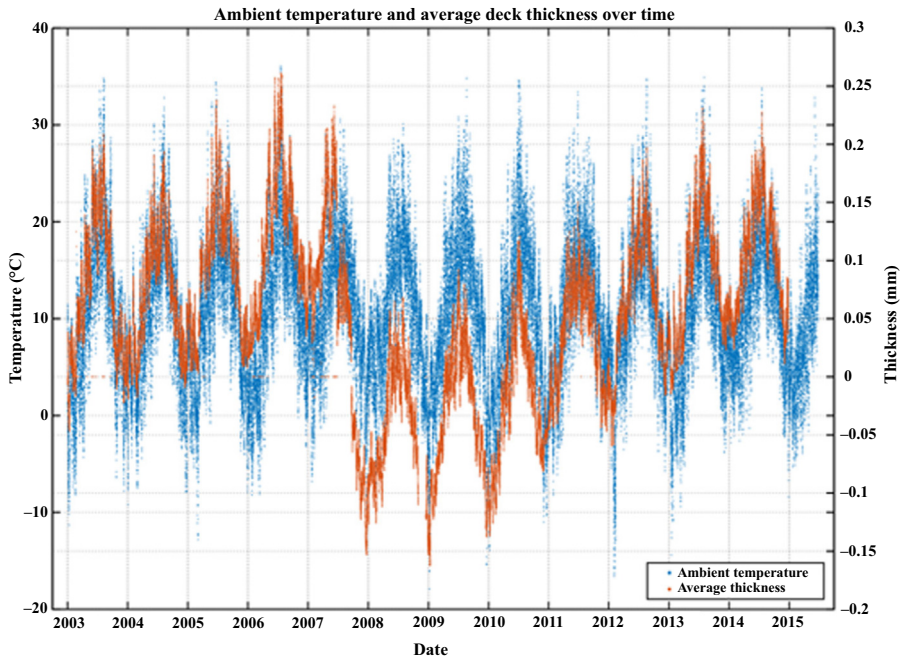


Figure 6.4 Relation between ambient temperature from Dutch meteorological institute and the average thickness of the deck over time.

6.3 Load test preparation

6.3.1 Visual inspection results

Six core tests were used to determine the concrete's properties (Witteveen + Bos, 2014). The results showed that the average cylinder concrete's compressive strength was 24 MPa, and the average cube's compressive strength was 44 MPa. No sample tests were used to determine the properties of the reinforcement steel. However, the symbols on the drawings show that smooth reinforcement bars were utilized. It is not stated on the drawings which steel grade was used, so these bars could be either steel grade QR22 (with a characteristic yield strength of 220 MPa) or QR24 (with a characteristic yield strength of 240 MPa), as these steel grades of plain bars were used in the 1960s. Fig. 6.5 depicts an overall view of the viaduct Zijlweg's reinforcement.

A visual inspection of the bridge was done before the field test. Fig. 6.6 shows the top deck's limited deterioration, which was only present at the sidewalk's edge during this inspection. As a result of the longitudinal expansion, the expansion joint between the deck and the abutment has shrunk considerably (see Fig. 6.7). It was decided to keep an eye on the expansion joint opening and closing during the proof load test in light of this problem. The ASR damage caused a typical cracking pattern (called map cracking) to appear on the slab. There was also evidence of cracking on the side faces. All cracking that was found and recorded is shown on the crack map in Fig. 6.8.

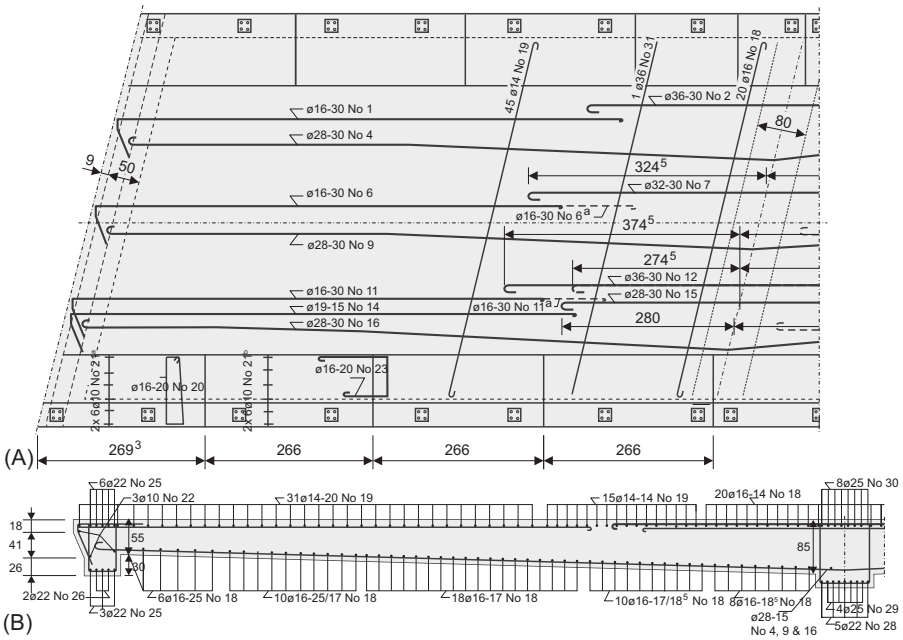


Figure 6.5 Reinforcement drawing: (A) top view; (B) side view. Bar diameters in (mm), all other dimensions in (cm).



Figure 6.6 Concrete deterioration of the sidewalk.

6.3.2 Loading positions and proof load magnitude

A proof load test is conducted on span 4 (Fig. 6.2), which is the northernmost span. The end span is used because it is not directly above the highway, which eliminates the



Figure 6.7 Closing of the expansion joint between the slab and the abutment.

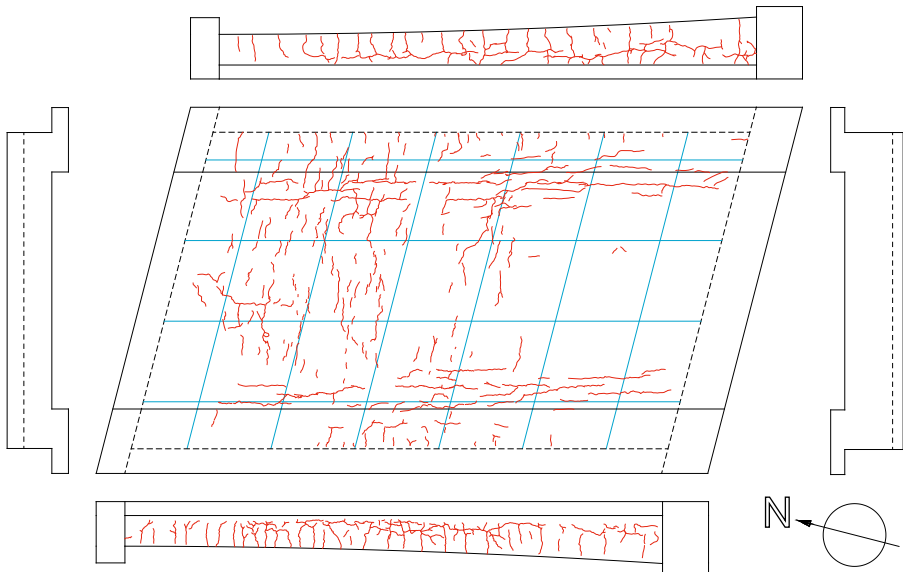


Figure 6.8 Map of cracks, showing bottom of slab and side faces.

need to close the highway while the test is being conducted and prevents any traffic obstructions for oncoming motorists. Over its length, span 4 has a variable thickness. Thickness of 550 mm is present at the end support. Near the mid support, the thickness parabolically increases to 850 mm. The parabola has a 150 m radius of curvature.

A linear finite element model is used to specify where the proof load should be applied. The sectional forces and moments in this model are identified. TNO Diana

(2012) is used. As the sidewalk's greater depth was not modeled, it was assumed that the slab's thickness in the transverse direction was uniform. To represent the additional self-weight from the sidewalk, additional dead load was instead applied in the model. Eight-node quadrilateral isoparametric flat shell elements were employed in the model. Instead of being 6.6 m wide, the slab is modeled to be 5.7 m wide (see Fig. 6.2 for geometry). The model included elements with dimensions of 500 mm in height and 483 mm in width. The element widths of the diaphragms at the intermediate supports and end supports are 410 and 250 mm, respectively. Each diaphragm uses elements with a height of 500 mm. Twelve elements are used in the transverse direction and 106 elements are used in the longitudinal direction of the final mesh. In the finite element model, supports are represented by the two elastomeric bearing pads. In the analysis report of the proof load test (Koekkoek et al., 2015), full details of the finite element model are available.

A load combination that includes the self-weight, dead load of the wearing surface, and loads from the live load model (distributed lane loads and concentrated live loads) is used to assess reinforced concrete slab bridges. The finite element model also uses these loads. Using a volumetric load of 25 kN/m^3 , the finite element model's geometry automatically generates the self-weight. The load at the edge, which results from the difference between the modeled 5.7 m and the actual 6.6 m width, is applied as 2.3 kN/m . In addition, a distributed load of 1.15 kN/m^2 is applied for the wearing surface of 46 mm of concrete. In addition, the superimposed dead load is an asphalt layer of 110 mm with a load of 23 kN/m^3 .

Load Model 1 from NEN-EN 1991-2:2003 (CEN, 2003) is used for the live loads. This load model contains per traffic lane a distributed lane load and concentrated wheel loads pertaining to a design tandem, as shown in Fig. 6.9. The wheel print of the design tandem is $400 \text{ mm} \times 400 \text{ mm}$, see Fig. 6.9. An axle load of $\alpha_{Q1} \times 300 \text{ kN}$ is applied in the first lane, of $\alpha_{Q2} \times 200 \text{ kN}$ in the second lane, and of $\alpha_{Q3} \times 100 \text{ kN}$ in the third lane. As the viaduct Zijlweg only has one lane, only $\alpha_{Q1} \times 300 \text{ kN}$ is applied. The values of α_{Qi} are nationally determined parameters, and these all take the recommended value of $\alpha_{Qi} = 1$ for the Netherlands. The lane load equals $\alpha_{q1} \times 9 \text{ kN/m}^2$ for the first lane, and $\alpha_{qi} \times 2.5 \text{ kN/m}^2$ for all lanes with $i > 1$. The values of α_{qi} are nationally determined parameters, and the value of $\alpha_{q1} = 1$ in the Netherlands when only one lane is present. The distributed lane load is applied over the width of the notional lane of 3 m, and pattern loading is used to find the most unfavorable loading arrangement. On the remaining width, $\alpha_{qr}q_{rk} = 2.5 \text{ kN/m}^2$ is applied with $\alpha_{qr} = 1$ and q_{rk} the distributed load on the remaining width of the viaduct, and on the sidewalk a pedestrian load of 5 kN/m^2 is applied. As the viaduct carries less than 250,000 vehicles per year, the reduction factors from NEN-EN 1991-2/NA:2011 (Code Committee 351001, 2011b) are used: 0.97 on the live loads from Load Model 1, and 0.90 on the remaining area, except for the pedestrian load on the sidewalk, for which no reduction factor can be used.

The wheel print from Load Model 1, see Fig. 6.9, is $400 \text{ mm} \times 400 \text{ mm}$. The finite element model uses shell elements, so that the loads are applied at mid-depth. Assuming a load distributed under 45 degree over the height, see Fig. 6.10, the load has to be distributed over $950 \text{ mm} \times 950 \text{ mm}$ in the finite element model, or 2 by 2 elements.

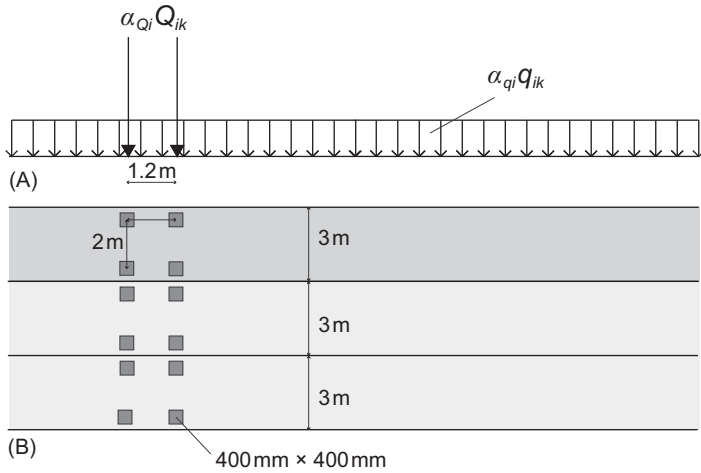


Figure 6.9 Live Load Model 1 from NEN-EN 1991–2:2003: (A) side view, (B) top view.

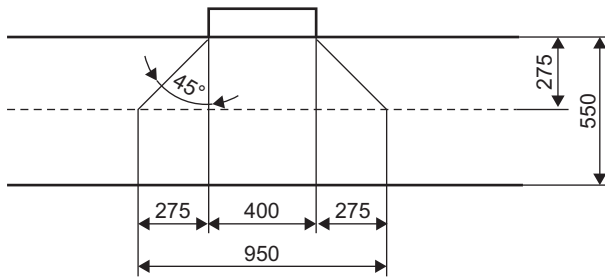


Figure 6.10 Distribution of wheel print over the depth.

As such, each wheel load of 150 kN becomes a distributed load of 0.155 N/mm². The tandem is centered in the notional lane of 3 m. As a result, the distance between the edge of the lane and the face of the first wheel in the transverse direction equals 500 mm. The wheel print of the proof load tandem is 230 mm × 300 mm, which better corresponds to the actual wheel print of a vehicle. Using the same assumptions as before (see Fig. 6.10) results in a loading surface in the finite element model of 780 mm × 850 mm.

The skew angle of the Zijlweg viaduct is 14 degrees. As a result, there are two ways that the position of the wheel prints is applied in the finite element model: parallel to the driving direction and following the width direction. The analysis revealed that for shear, the position along the width is more crucial, while for bending moments, applying loads parallel to the driving direction results in the largest load effect.

The safety levels applied in the Netherlands are described in NEN-EN 1990:2002 (CEN, 2002) for new structures and in NEN 8700:2011 (Code Committee 351001, 2011a) for existing structures. The Guidelines for the Assessment of Bridges

(“RBK,” RTD 1006:2013) (Rijkswaterstaat, 2013) have additional requirements for existing highway bridges. Table 6.1 provides an overview of these safety levels, along with the corresponding reliability index and reference period. A different load combination, as shown in Table 6.2, is used when evaluating a bridge using a proof load test. The load factor for the self-weight changes to 1.10 for this load combination. The self-weight can be thought of as a deterministic value for an existing structure. The only remaining component is the model factor, which in NEN-EN 1991–2 C1:2011 (CEN, 2011) is 1.07. The value of 1.1 can be used to round off this value. Therefore, the load factors γ_{sw} , γ_{sd} , and γ_{LL} from Table 6.2 are used for an assessment using the load combination with the Eurocode live loads, while γ_{sw} , γ_{sd} , and γ_{proof} from Table 6.2 are used for preparations for a proof load test.

The critical position for the bending moment test is sought first to determine the necessary load on the proof load tandem. To achieve this, the design tandem of the Eurocode is moved along the span (parallel to the driving direction) until the position that produces the largest sectional moment is found. Following the removal of the Eurocode live loads from the model, the proof load tandem is applied at the critical position in the model. The load is then increased on the proof load tandem until the

Table 6.1 Overview of safety levels for new and existing structures in the Netherlands, with their respective load factors.

| Safety level | β | Reference period (years) | γ_{sw} | γ_{sd} | γ_{LL} |
|--------------------|---------|--------------------------|---------------|---------------|---------------|
| ULS Eurocode | 4.3 | 100 | 1.35 | 1.35 | 1.50 |
| RBK Design | 4.3 | 100 | 1.25 | 1.25 | 1.50 |
| RBK Reconstruction | 3.6 | 30 | 1.15 | 1.15 | 1.30 |
| RBK Usage | 3.3 | 30 | 1.15 | 1.15 | 1.25 |
| RBK Disapproval | 3.1 | 15 | 1.10 | 1.10 | 1.25 |
| SLS Eurocode | 1.5 | 50 | 1.00 | 1.00 | 1.00 |

β , The associated reliability index; γ_{sw} , the load factor on the self-weight; γ_{sd} , the load factor on the superimposed load; γ_{LL} , the load factor on the live load.

Table 6.2 Load factors used in combination with a proof load test at the different safety levels.

| Safety level | γ_{sw} | γ_{sd} | γ_{LL} | γ_{proof} |
|--------------------|---------------|---------------|---------------|------------------|
| ULS Eurocode | 1.10 | 1.35 | 1.50 | 1.00 |
| RBK Design | 1.10 | 1.25 | 1.50 | 1.00 |
| RBK Reconstruction | 1.10 | 1.15 | 1.30 | 1.00 |
| RBK Usage | 1.10 | 1.15 | 1.25 | 1.00 |
| RBK Disapproval | 1.10 | 1.10 | 1.25 | 1.00 |
| SLS Eurocode | 1.00 | 1.00 | 1.00 | 1.00 |

γ_{sw} , The load factor on the self-weight; γ_{sd} , the load factor on the superimposed load; γ_{LL} , the load factor on the live load; γ_{proof} , the load factor for the proof load tandem.

same sectional moment as with the Eurocode load combination is obtained. At a face-to-face distance of 3382 mm (seven elements) between the support and the tandem, the critical position for bending moment is found in span 4 of the viaduct Zijlweg. The target proof load is determined by the corresponding safety level. In Table 6.3, under the heading $P_{tot,bending}$, are the calculated values for the target proof loads.

For shear, the critical position is known to be at a face-to-face distance of $2.5 d_l$ between the load and the support (Lantsoght et al., 2013b), with d_l the effective depth to the longitudinal reinforcement. An overview of the finite element model is given in Fig. 6.11. This critical distance is derived from slab shear experiments in the laboratory (Lantsoght et al., 2013c, 2014, 2015a,b,c). This distance, however, has been derived for straight slabs, and the behavior of skewed reinforced concrete slabs in shear requires further research. Limited testing showed that the behavior of skewed slabs in shear is complex and that the failure mode changes as the skew angle changes (Cope et al., 1983; Cope, 1985). It is known that the obtuse corner results in

Table 6.3 Required target proof loads for different safety levels, for bending moment and shear.

| Safety level | $P_{tot,bending}$ (kN) | $P_{tot,shear}$ (kN) |
|--------------------|------------------------|----------------------|
| ULS Eurocode | 1259 | 1228 |
| RBK Design | 1257 | 1228 |
| RBK Reconstruction | 1091 | 1066 |
| RBK Usage | 1050 | 1027 |
| RBK Disapproval | 1049 | 1025 |
| SLS Eurocode | 815 | 791 |

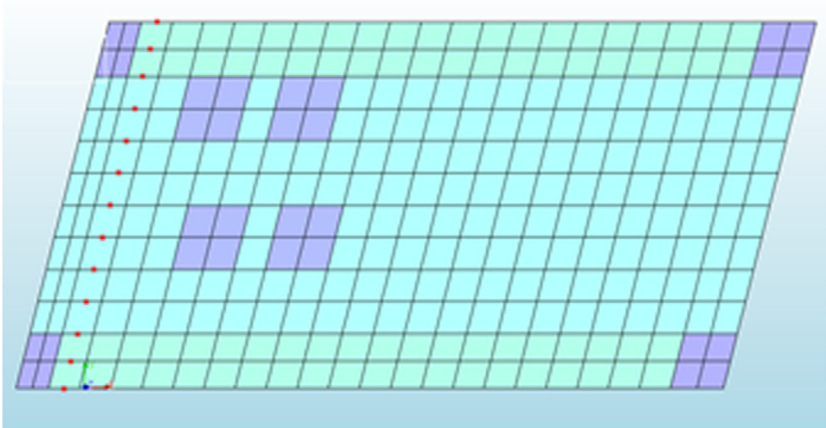


Figure 6.11 Overview of finite element model with critical position for shear.

the largest concentrations of shear stresses, so that the critical position is with the tandem in the obtuse corner. The peak shear stress in the linear finite element model can be distributed over $4 d_l$, as was derived based on the comparison between linear finite element models and measurements of the support reaction for slabs (Lantsoght et al., 2013a). This averaged shear stress is then used for the analysis and for comparison between the shear stress caused by the load combination prescribed by the code and the load combination with the proof load tandem. Both the design tandem and the proof load tandem are placed at a face-to-face distance of $2.5 d_l$ from the support. First, the sectional shear (averaged over $4 d_l$) is determined caused by the load combination prescribed by the code. Then, the required proof load to get the same sectional shear (averaged over $4 d_l$) is determined. The proof load tandem is placed in the obtuse corner, which is known from the literature (Cope, 1985) to lead to the largest concentrations of shear stresses. Finite element models were made to study the difference for the viaduct Zijlweg between loading at the acute and obtuse corner. It was indeed confirmed that the critical position is in the obtuse corner (Koekkoek et al., 2015). Finally, the results of the target proof loads for shear $P_{tot,shear}$ for the different safety levels are determined, as shown in Table 6.3. It must be mentioned that proof load testing for shear is generally not permitted by the existing codes and guidelines and that the development of stop criteria for a proof load test for shear is still subject of research (Schacht et al., 2016a). Recent research at the Delft University of Technology uses laboratory testing to develop shear stop criteria, with the aim of developing safe procedures for proof load testing of shear-critical structures (Christensen et al., 2022; Zarate Garnica et al., 2021; Zarate Garnica and Lantsoght, 2019, 2020, 2021; Zárate Garnica, 2018; Yang et al., 2018).

The position of the load is slightly altered from the critical position established using the finite element models during the execution of the proof load test for practical reasons. To partially maintain the loading setup constructed for the test, the centerline for the bending moment test is kept the same as it is for the shear test. Thanks to this adjustment, the supports can stay in place, and the load spreader beams, jacks, and load cells are moved between the two experiments.

6.4 Report of load test

6.4.1 Loading protocol

On Wednesday, June 17, 2015, the viaduct Zijlweg underwent two proof load tests. All measurement tools were brought to the test site on Sunday, June 14th. The sensors were applied on Monday and Tuesday morning, and on Tuesday afternoon, all sensors were tested.

A cyclic loading protocol was applied in the proof load test, as recommended in the German load testing guidelines and in ACI 437.2M-14. German load testing guidelines (Deutscher Ausschuss für Stahlbeton, 2000) state that each load test must be performed in at least three steps, with the maximum load in each step remaining constant for at least 2 minutes. A cyclic loading protocol's advantage

(Koekkoek et al., 2016) is that the measurements' reproducibility, symmetry, and linearity can be independently confirmed. Four load levels were chosen for testing the Zijlweg viaduct:

1. A low load level of about 40 metric tons to ensure that all sensors are operating properly. Prior to performing the proof load test, adjustments can be made if a sensor is found to be malfunctioning. Both the shear test and the bending moment test required one LVDT to be placed within its measurement range and corrections for the load cells at the first load level.
2. The load level of the Serviceability Limit State. Large deflections or cracks are not anticipated at this load level, and the behavior should be linear elastic. The measurements are interpreted to determine whether it is safe to load to the next load level before moving on to it.
3. An intermediate load level to build up to the target proof load. It is determined whether the testing can go on based on the closely monitored measurements and the observed structural response.
4. The target proof load for the RBK design level magnified by 5% from Table 6.3. Cycles are not necessary at this load level because it is not necessary to interpret the stop criteria or the linearity of the measurements to determine whether additional loading is permitted. The extra loading of 5% is used to account for the material's variability and the fact that only two positions are tested. Note that further research on the probabilistic substantiation of proof load testing is underway to check, among others, if the 5% extra loading is necessary.

The load is not lowered to 0 tons after each load cycle; instead, a threshold value of 10 tons is used. Due to the sensitivity of acoustic emission measurements to full unloading, this minimum load level ensures that all sensors and jacks remain active while also preventing unwanted noise. During the load test, it was important to maintain a constant loading speed. However, since the speed was chosen manually, some variations happened. Fig. 6.12 depicts the proof load tandem's position during the bending moment test, and Fig. 6.13 depicts its position during the shear test.

6.4.2 Instrumentation

Sensors are positioned at various points on the slab's bottom face, side faces, and the joint to monitor the bridge's various responses during the proof load test. Fig. 6.14 presents a general overview of the instrumentation. On the measurement computer in the control center on site, all measured data are displayed in real time. Every time a load cycle is completed, these measurements are interpreted and the findings are used to decide whether additional loading is acceptable. During the proof load tests, the following structural responses are monitored:

- slab deflections,
- cross-beam deflections,
- crack widths,
- bottom slab strains,
- end support rotation,
- acoustic emission signals,
- joint opening,
- side face crack opening (no real-time monitoring).

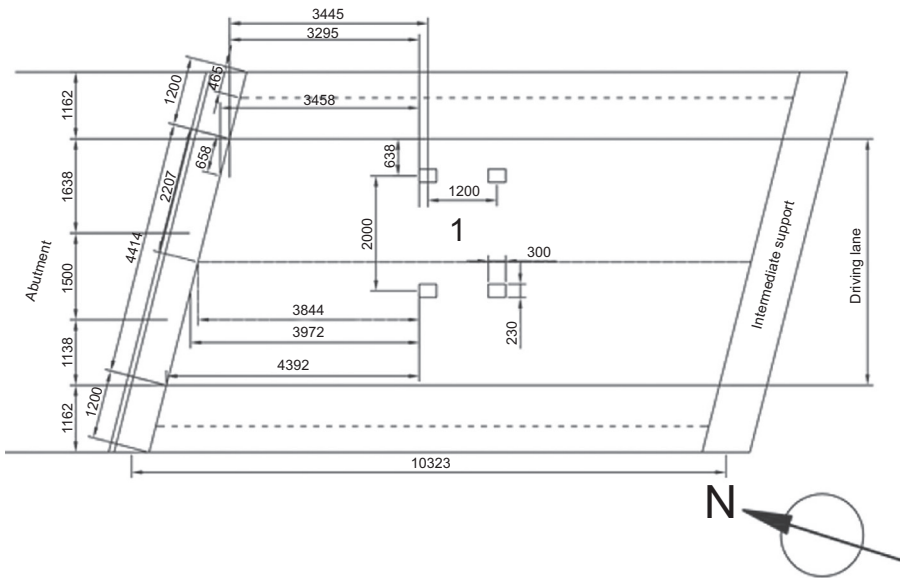


Figure 6.12 Position of proof load tandem for the bending moment test.

Laser distance finders (lasers) and linear variable differential transformers (LVDTs) are used to measure these responses. For monitoring of the side face crack opening, we applied gypsum over the crack and checked later to see if it has cracked, which would indicate that the crack was activated during the test. [Table 6.4](#) provides an overview of the used sensors. The analysis of the acoustic emission measurements is presented in a separate report ([Yang and Hordijk, 2015](#)). Recent advances in the determination of stop criteria during proof load testing are detailed in ([Zhang, 2022](#)). Verification of these proposals in a field test is a topic of further research.

Utilizing data collected by LVDTs and laser distance finders, the vertical displacement of the deck is determined. To ascertain the longitudinal deflection profiles, a row of four LVDTs is positioned in the middle of the hypothetical lane. To account for how the measurement frame is applied, a second LVDT, which is attached to the slab at the mid support but resting on the abutment at the end support, is used. Two lasers are used to create the transverse deformation profiles, and they are placed halfway between the locations of the wheel prints used for the bending moment test and the shear test. By measuring the deflections, the deflection profiles in the transverse and longitudinal directions can be set up, the load-deflection diagram can be followed in real time throughout the experiment, and residual deflections can be calculated after each load step. Existing codes ([Deutscher Ausschuss für Stahlbeton, 2000](#); [ACI Committee 437, 2013](#)) set limits on the residual deflection as a stop or acceptance criterion and recommend the use of the load-deflection diagram to identify nonlinearity. [Fig. 6.15](#) gives a summary of the deflections being measured using LVDTs and lasers. Lasers (two per support) are used

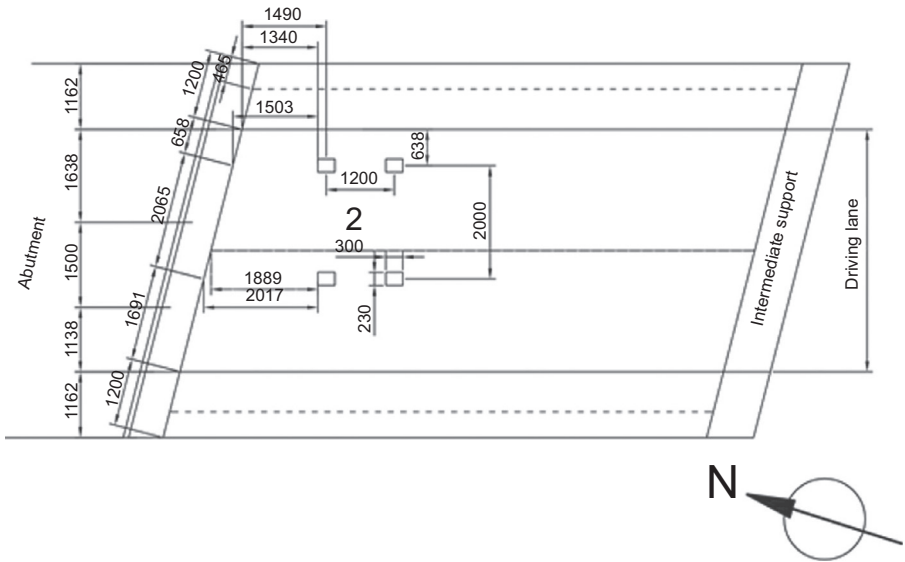


Figure 6.13 Position of proof load tandem for the shear test.

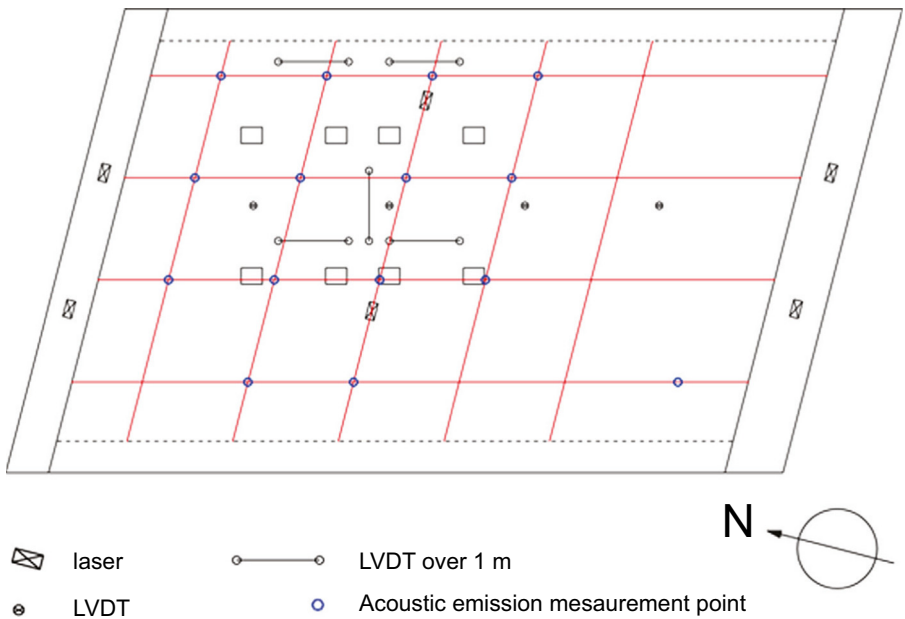


Figure 6.14 Overview of applied sensors.

Table 6.4 Overview of applied sensors, measurement range, and their application.

| Name | Range (mm) | Application |
|--------|------------|---|
| LVDT1 | 10 | Strain over 1 m |
| LVDT2 | 10 | Strain over 1 m |
| LVDT3 | 10 | Strain over 1 m |
| LVDT4 | 10 | Reference for change in temperature |
| LVDT5 | 20 | Deflection of the slab (on a longitudinal line) |
| LVDT6 | 20 | Deflection of the slab (on a longitudinal line) |
| LVDT7 | 20 | Deflection of the slab (on a longitudinal line) |
| LVDT8 | 20 | Deflection of the slab (on a longitudinal line) |
| LVDT9 | 10 | Displacement of the joint |
| LVDT10 | 10 | Displacement of the joint |
| LVDT11 | 10 | Displacement of the joint |
| LVDT12 | 10 | Displacement of the joint |
| LVDT13 | 10 | Deflection of the slab (on a longitudinal line) |
| LVDT14 | 10 | Crack width |
| LVDT15 | 10 | Crack width |
| LVDT16 | 10 | Crack width |
| Laser1 | 100 | Deflection of the slab (on a transverse line) |
| Laser2 | 20 | Deflection of the slab (on a transverse line) |
| Laser3 | 20 | Deformation of support (N) |
| Laser4 | 20 | Deformation of support (N) |
| Laser5 | 100 | Deformation of support (S) |
| Laser6 | 100 | Deformation of support (S) |

to measure the vertical displacement of the cross beams at the end support and mid support. The compression of the elastomeric bearings used for the supports leads to the deflection of the cross-beam. Fig. 6.16 depicts the placement of these measurements.

Both an existing crack and a crack that forms during the proof load test can have their widths measured. The challenge is predicting which crack will open during the test. LVDTs are positioned horizontally over the crack to measure the expansion of the crack's width. Existing cracks were monitored throughout proof load tests on the Zijlweg viaduct. Prior to the proof load test, two cracks—one longitudinal and one transverse—were picked out for monitoring. The German recommendation establishes a maximum crack width during a proof load test as well as a maximum residual crack width that must be confirmed following each load step. Fig. 6.17 displays a diagram of the locations of the LVDTs used to measure crack width. Current research focuses on the use of DIC (digital image correlation) to follow multiple cracks during proof load testing (Zhang et al., 2020; Christensen et al., 2021, 2022; Halding et al., 2018).

Applying an LVDT horizontally over 1 m will measure the deformation on the slab's bottom, from which the strain can be calculated. Three LVDTs are used to calculate strains, and a reference LVDT is placed on a section of the bridge that is not loaded during the load test to evaluate the impact of temperature and humidity. It is

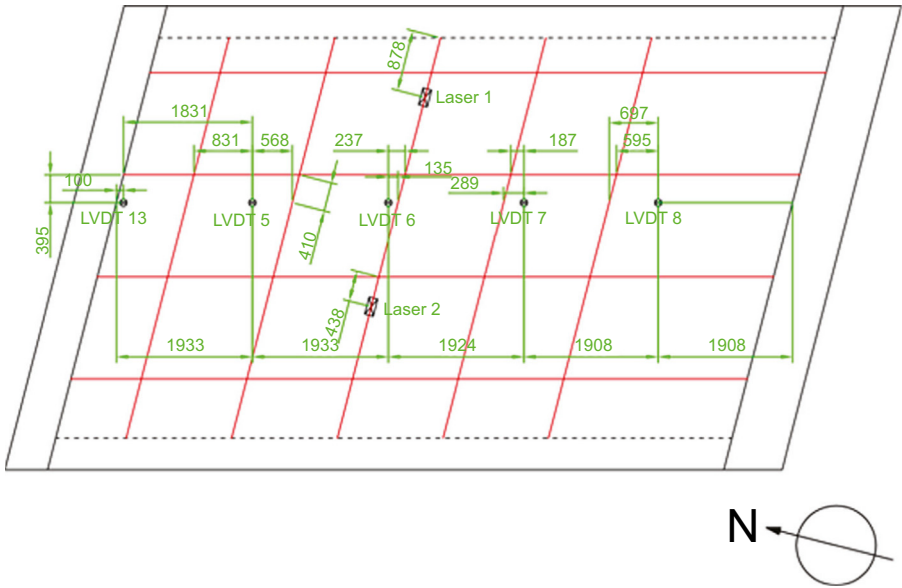


Figure 6.15 Applied sensors for measuring deflections of the slab.

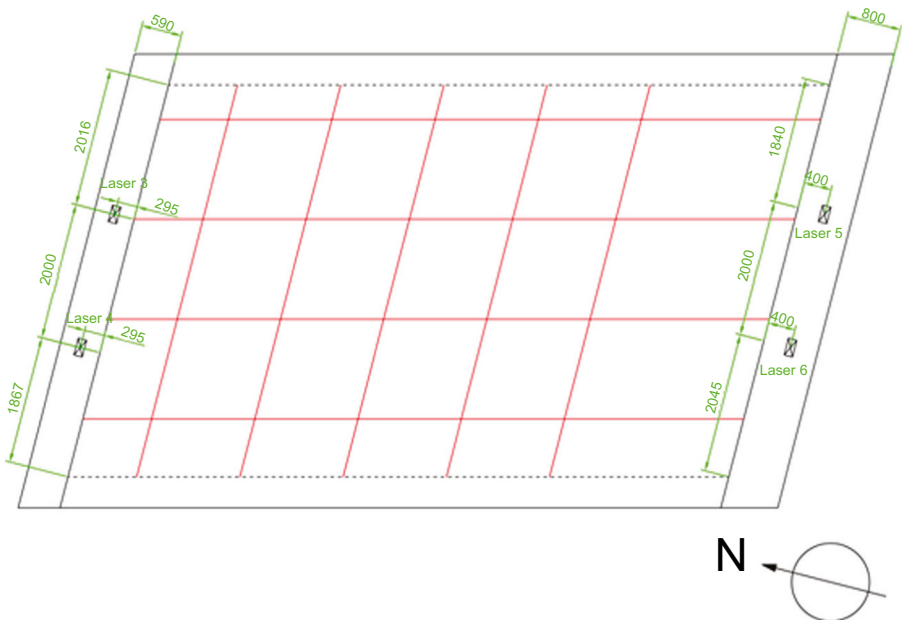


Figure 6.16 Applied lasers for measuring deflections of the cross-beams.

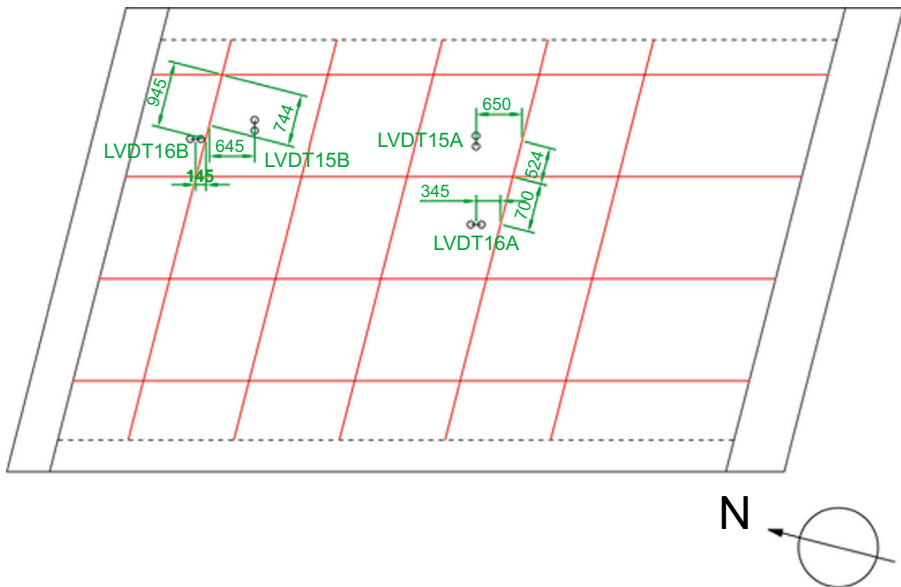


Figure 6.17 Applied LVDTs for measuring the crack widths during the test. Position “A” is the bending moment test, and position “B” is the shear test. *LVDTs*, Linear variable differential transformers.

crucial to account for temperature (and humidity) effects because the LVDT support construction is made of aluminum, which has a high coefficient of thermal expansion. A limiting concrete strain is recommended as a stop criterion in the German guideline. As a result, during the experiment, it is necessary to pay attention to the strain. During the proof load test, a new crack that forms inside the 1 m that the strain LVDT measures will also be measured. Fig. 6.18 provides an overview of the tree strain LVDTs.

Less room was left for the joint as a result of the viaduct’s longitudinal expansion brought on by the alkali-silica reaction. Two LVDTs are installed on either side of the joint to measure joint movement and end support rotation as well as to determine if there is ever a load for which the expansion joint is left with insufficient room or if the required rotation of the bridge deck during proof load tests is restricted, as this would change the bending moment line. The joint is horizontally measured by the LVDTs. The slab and the abutment are connected to opposite ends of the LVDT. Fig. 6.19 depicts how the LVDTs are arranged on the joint at the west side of support 5. LVDTs are applied to the east side in the same locations as they are on the west side; the only distinction is that the east side uses LVDTs numbers 11 and 12.

Finally, we used four different load cells to measure the applied load at each of the four wheel prints during the proof load test. The load cells are accurate to 1% (10 kN) and have a capacity of 1000 kN. During the proof load test, the load measurements are crucial because they are used to follow the load-deflection diagram in real time. One of the stop criteria is violated when the load-deflection diagram stops being linear.

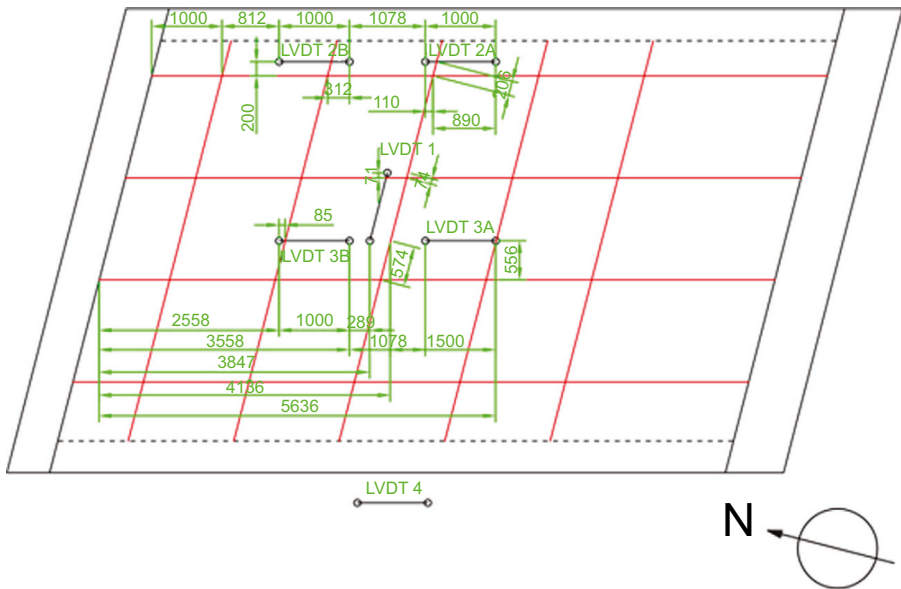


Figure 6.18 Applied LVDTs for measuring strains during the test (not showing the reference LVDT). Position “A” is the bending moment test, and position “B” is the shear test. *LVDTs*, Linear variable differential transformers.

6.5 Analysis of load test

6.5.1 Test results

The proof load test results at the flexure-critical position are reviewed first. A total of 1332 kN was the highest load that could be measured on the proof load tandem. A total load of 1368 kN is the final result, from adding the weight of the steel plate and jacks to the externally applied load. The measured load on the four jacks is used to create the envelope of the load–displacement diagram, which is used to evaluate if nonlinearity occurs. Fig. 6.20 shows the envelope for the load–deflection diagram. The stiffness, or tangent to the load–deflection diagram, is represented by the black lines. Nonlinear behavior is seen when the angle of the black lines reduces significantly. While the behavior for the final loading and unloading step was stiffer in the unloading branch, the stiffness has only slightly decreased in the third black line. This stiffening may be brought on by transverse stress redistribution at higher loads, interaction between the applied loading frame and the structural behavior of the bridge, or the slower loading speed in the final loading step. No nonlinearity was observed.

Plots of the deflection in the span direction at various load steps are created using the longitudinal line of LVDTs. As can be seen in Fig. 6.21, in which the axes of the proof load tandem are also shown, the results of the deflection plots are consistent with expectations. The largest deflections are measured by the LVDT

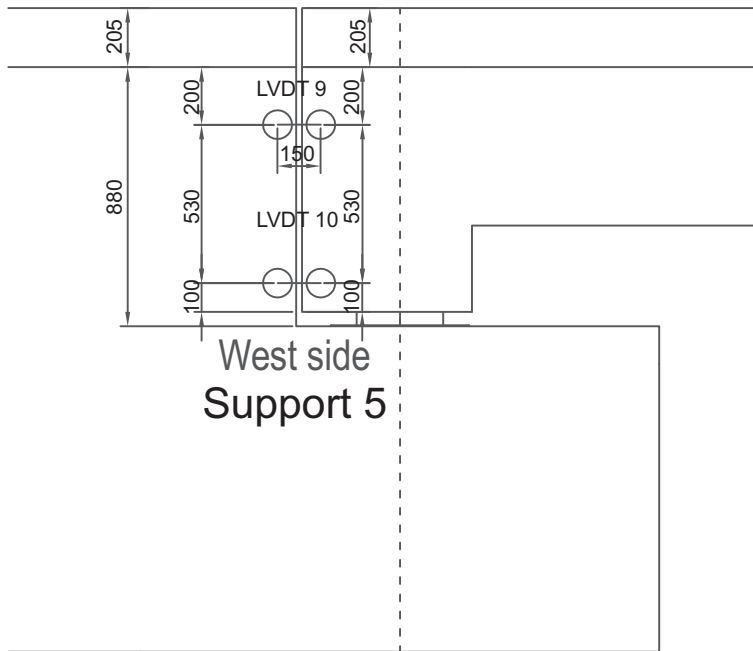


Figure 6.19 Position of LVDTs that measure joint opening and rotation, on the west side of the support. The east side is symmetric. *LVDTs*, Linear variable differential transformers.

under the center of the proof load tandem, as expected. The transverse direction measurements can produce a deflection plot that looks similar, as shown in Fig. 6.22. The measurement point closer to the sidewalk deflects more in the transverse direction at lower load levels and less at higher load levels. The behavior is less stiff at low load levels because of the observed cracking on the slab's side facing the sidewalk, which is one explanation for this observation. Because there are stirrups in the sidewalk, the increased stiffness at higher loads makes sense. All of the measured strains are fully linear.

We instrumented three existing cracks during the proof load test. A transverse crack was measured by LVDT 16, a longitudinal crack at the slab's bottom was measured by LVDT 15, and a shear crack that could become critical was measured by LVDT 14. Fig. 6.23 shows a plot of the test results for the crack width at various load levels. This diagram demonstrates how the test did not cause the potential shear crack to open up. The longitudinal crack exhibits small and linear behavior. We observed less activation of the longitudinal crack than of the transverse crack. Note that there were no indications of nonlinearity and that the largest increase in crack width for all measured cracks was extremely small. Fig. 6.24 depicts the outcomes of the measurements made on the reference LVDT. These strains are contrasted with the ambient temperature, which was determined using data from a location 14 km south of the load testing site provided by the Dutch Royal

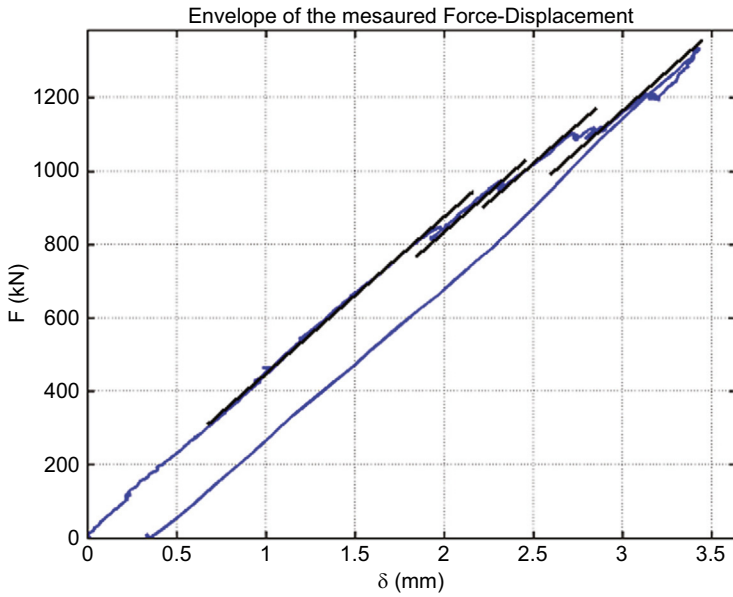


Figure 6.20 Envelope of load–displacement diagram for the bending moment test. The black lines indicate the tangent to the diagram, that is, the stiffness.

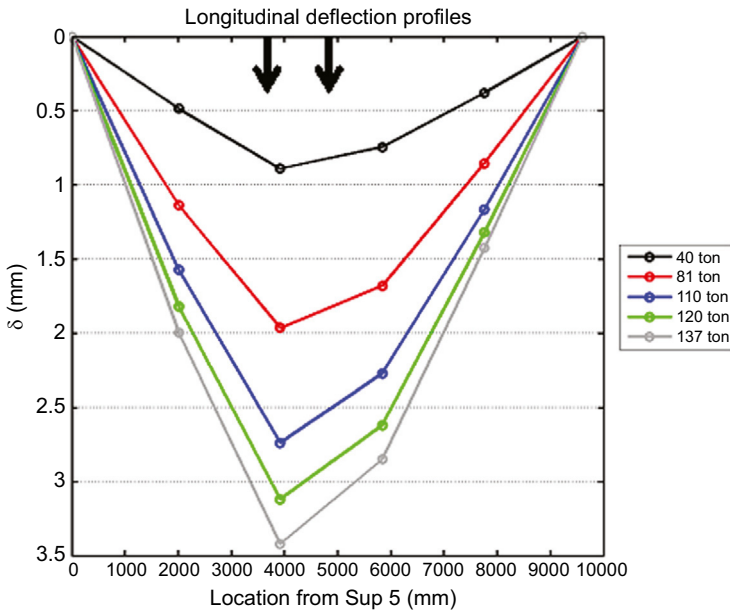


Figure 6.21 Deflection plots in the longitudinal direction for the bending moment test, indicating the position of the proof load tandem.

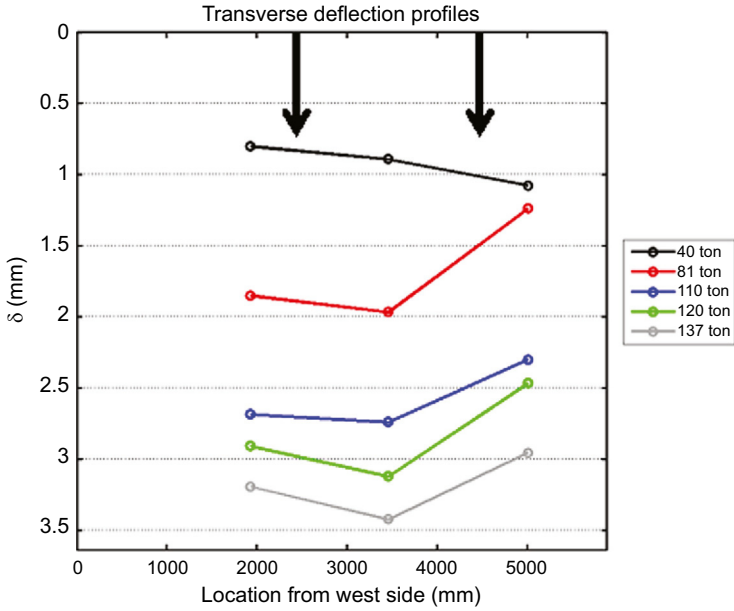


Figure 6.22 Deflection plots in the transverse direction for the bending moment test, indicating the position of the proof load tandem.

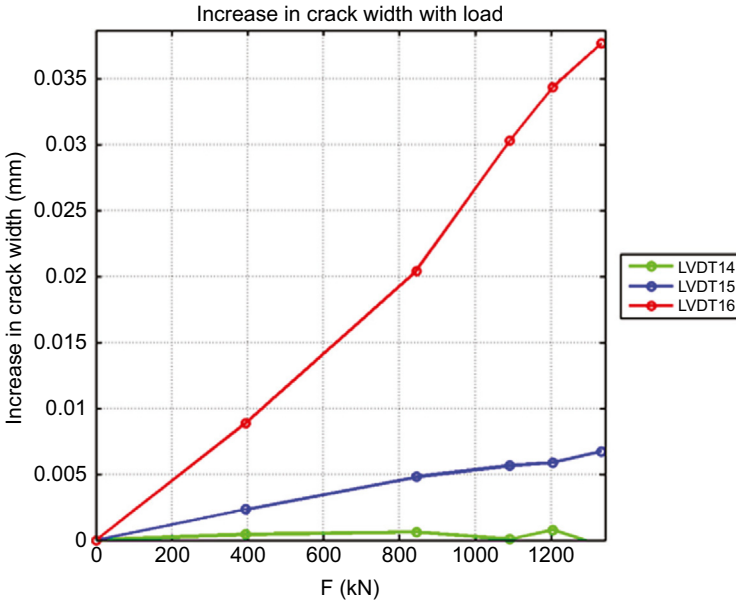


Figure 6.23 Measured crack width for selected load levels during the bending moment test.

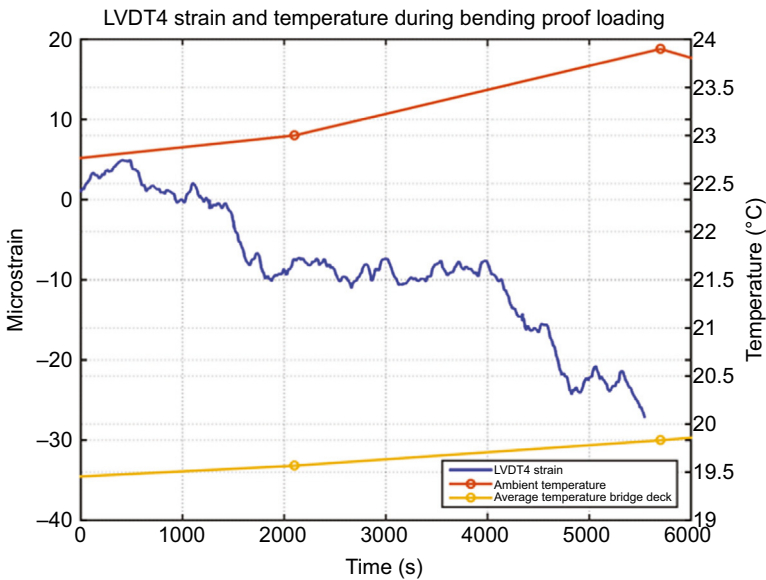


Figure 6.24 Strain measured by LVDT4 during the bending moment test, compared to ambient temperature and average temperature of bridge deck. *LVDTs*, Linear variable differential transformers.

Meteorological Institute (KNMI, 2015), and with the measured bridge deck temperature, which was determined with the ASR monitoring system. It is clear that the behavior of the bridge deck's temperature and the ambient air temperature (14 km further south) is comparable. The strain is inversely proportional to the temperature. LVDT compression and aluminum strip elongation, both of which are brought on by an increasing temperature, are represented by a reduction of the measured strain. As a result, the outcomes for the strains are in line with our expectations, and these values are used to correct the strains that were measured at the slab's bottom to reflect the net strain under the applied proof load.

The second test to discuss is the proof load test at a shear-critical position. Fig. 6.25 shows the loa–deflection diagram. The proof load test for shear's maximum applied load was 1342 kN, and when the weight of the jacks and the steel plate are accounted for, the maximum load of 1377 kN results. The measured behavior is fully linear, and no evidence of nonlinearity is found, as can be seen from the load–deflection diagram (Fig. 6.25). In Fig. 6.26, the deflection plots in the longitudinal direction are displayed. All outcomes are as anticipated, with the exception of the last measurement point. A more in-depth analysis of this LVDT's output revealed that between 600 and 1100 kN, the results were suddenly shifted to larger values, before being shifted back to smaller values. This observation can be explained by the possibility that the LVDT was outside of its measurement range, fully compressed and only able to move slightly in response to temperature changes in the aluminum measurement frame. Fig. 6.27 shows the deflection plot in the

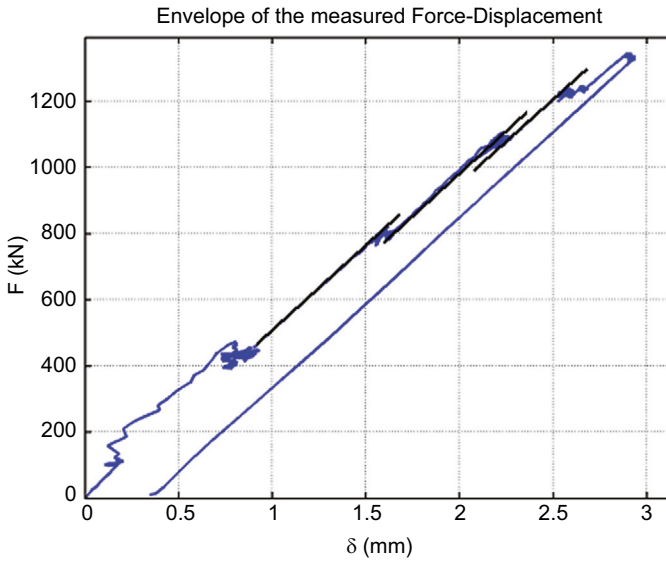


Figure 6.25 Envelope of load-displacement diagram for the shear test. The black lines indicate the tangent to the diagram, that is, the stiffness.

transverse direction, which is also as anticipated. Due to the shear reinforcement and consequently slightly stiffer behavior of the sidewalk, the deflection under the sidewalk is marginally less than the deflection in the span. All measured strains are completely linear. Once more, three existing cracks were monitored during the test. LVDT 14 was placed over a potential shear crack at the same location as during the bending moment test, LVDT 15 over a longitudinal crack on the bottom face, and LVDT 16 over a transverse crack on the bottom face. Fig. 6.28 illustrates how the applied load causes the cracks' widths to increase. It is obvious that all monitored cracks are only minimally activated (the largest crack width is less than 0.025 mm). Concerns about the structural integrity of the tested bridge were unfounded because the possible shear crack's increase in crack width was slight and linear. The experiment did not result in the joint closing completely or causing rotation, and the temperature effect was as noted for the bending moment test.

6.5.2 Overview of available stop criteria

In the German guideline ([Deutscher Ausschuss für Stahlbeton, 2000, 2020](#)), stop criteria are defined. The stop criteria from the German guideline can be used for flexure in plain and reinforced concrete buildings.

The first stop criterion from the German guideline says that the ratio of the residual to maximum deformation is limited to 10%. The second stop criterion from the German guideline considers the strains in the steel. Typically, a bridge owner might not allow the removal of the concrete cover to measure the steel strains. Therefore,

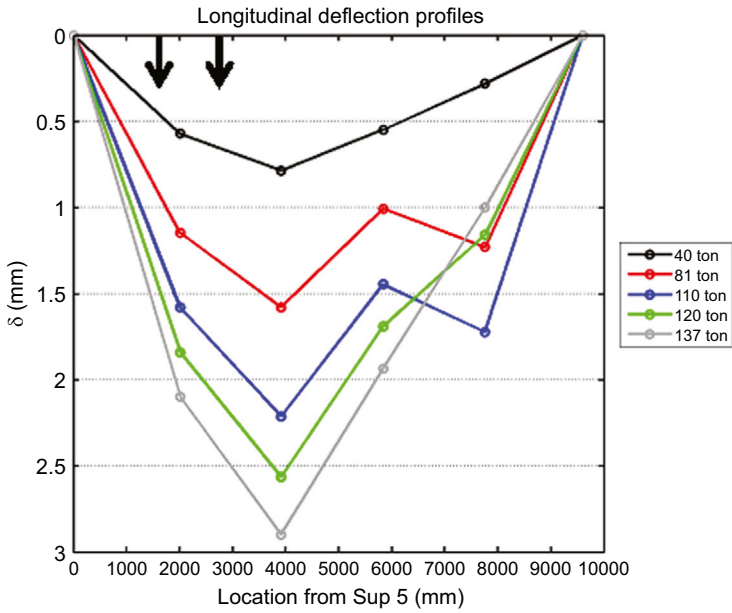


Figure 6.26 Deflection plots in the longitudinal direction for the shear test, also indicating the position of the proof load tandem.

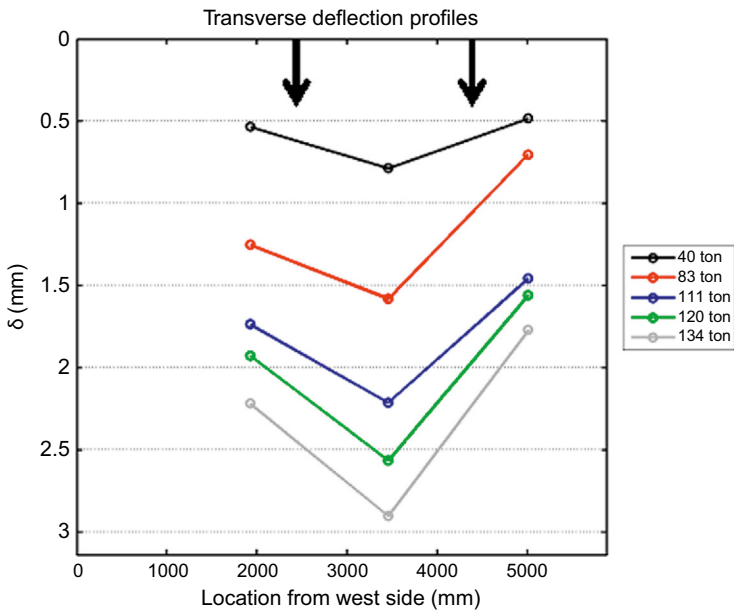


Figure 6.27 Deflection plots in the transverse direction for the shear test, also indicating the position of the proof load tandem.

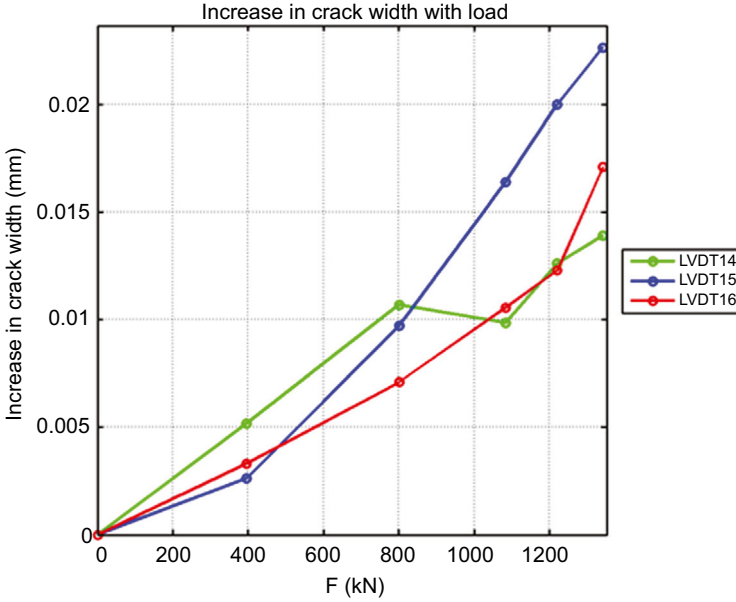


Figure 6.28 Measured crack width for selected load levels during the shear test.

this stop criterion is considered as not practical. The third stop criterion considers the strains measured in the concrete. This stop criterion is formulated as follows:

$$\varepsilon_c < \varepsilon_{c,lim} - \varepsilon_{c0} \quad (6.1)$$

with ε_c the measured strain in the concrete, $\varepsilon_{c,lim}$ the limiting strain of $800 \mu\varepsilon$, and ε_{c0} the strain caused by the permanent loads. The last stop criterion from the German guideline is related to crack width. The guideline has different requirements for existing cracks and newly developed cracks. The first requirement is that the maximum crack width increase during the proof load test, $\Delta w \leq 0.3 \text{ mm}$. The second requirement considers the residual crack width, after a load cycle, for which holds that the value of the residual crack width $\leq 0.2 \times \Delta w$.

Based on research on beams in the laboratory, we have proposed a set of stop criteria for shear and flexure (Lantsoght et al., 2018c). For flexure (Lantsoght et al., 2019c), the limiting strain is proposed as:

$$\varepsilon_c \leq \varepsilon_{c,bot,max} - \varepsilon_{c0} = \varepsilon_{stop} \quad (6.2)$$

with ε_c the measured strain in the concrete, $\varepsilon_{c,bot,max}$ the limiting strain derived from sectional equilibrium, and ε_{c0} the strain caused by the permanent loads. The value of $\varepsilon_{c,bot,max}$ is based on maximum 65% of the yield strain in the steel:

$$\varepsilon_{c,bot,max} = \frac{h - c}{d - c} \times \frac{0.65f_{ym}}{E_s} \quad (6.3)$$

where h is the height of the cross-section, c is the height of the concrete compression zone that corresponds to a stress of $0.65f_{ym}$ in the reinforcement steel (which can be determined from sectional equilibrium using, for example, Thorenfeldt's parabolic stress–strain relation), f_{ym} is the average yield strength of the reinforcement steel, and E_s is the Young's modulus of the reinforcement steel. The limiting crack width in this proposal is proposed as:

$$w_{stop} = 2 \frac{0.65f_{ym} - f_{perm}}{E_s} \beta_{fr} \sqrt{d_c^2 + \left(\frac{s}{2}\right)^2} \quad (6.4)$$

In this expression, d_c is the concrete cover to the centroid of the tension steel, s the reinforcement spacing, and β_{fr} the strain gradient term, given as:

$$\beta_{fr} = \frac{h - c}{d - c} \quad (6.5)$$

where d is the effective depth of the reinforcement. The stress caused by the permanent loads f_{perm} is determined as:

$$f_{perm} = \frac{d - c}{h - c} \varepsilon_{c0} E_s \quad (6.6)$$

In addition to these stop criteria for strain and flexure, we propose to neglect all cracks that are smaller than 0.05 mm, as such small crack widths are not related to structural cracking. The limit for the residual crack width w_{res} as a function of the maximum crack width w_{max} is taken from the German guideline (as described previously). To limit nonlinearity, we propose to limit the reduction of the stiffness determined in the load–deflection diagram to a maximum of 25%. We also propose to qualitatively monitor the deformation profiles in the transverse and longitudinal direction during the test and to monitor the overall load–deflection diagram. These qualitative stop criteria require engineering judgement and an interpretation of the overall structural behavior.

For shear, we have proposed a series of stop criteria, but are currently still carrying out research on slab specimens to develop better shear stop criteria. A validation of the newly developed shear stop criteria in a field test is also still a topic of future research. The first proposed shear stop criterion is based on the strain in the concrete and is based on the Critical Shear Displacement Theory (CSDT) (Yang et al., 2017, 2016):

$$\varepsilon_{lim,CSDT} = \varepsilon_{c,bot,max} - \varepsilon_{c0} \quad (6.7)$$

where and $\varepsilon_{c,bot,max} = 0.65 \cdot \varepsilon_{c,bot,CSDT}$. To determine these parameters, we first define the shear capacity according to the CSDT as V_{CSDT} :

$$V_{CSDT} = V_c + V_d + V_{ai} \quad (6.8)$$

where the contribution from the concrete in the compression zone V_c is based on a linear stress distribution and the residual stresses in the crack are neglected (Morsch, 1922):

$$V_c = \frac{2z_c}{3z} V = \frac{d - s_{cr}}{d + 0.5s_{cr}} V \quad (6.9)$$

where z is the length of the lever arm between the equivalent compressive force and the tension force in tensile reinforcement, z_c is the height of the uncracked zone at the tip of the major crack, d is the effective depth, V is the shear force, and s_{cr} is the height of a fully developed crack:

$$s_{cr} = \left[1 + \rho_s n_e - \sqrt{2\rho_s n_e + (\rho_s n_e)^2} \right] d \quad (6.10)$$

with ρ_s the reinforcement ratio and n_e the ratio between the Young's modulus of the steel (E_s) and the Young's modulus of the concrete (E_c). The contribution of dowel action, V_d , is determined as (Baumann and Rusch, 1970):

$$V_d = 1.64b_n\varphi^3\sqrt{f_c} \quad (6.11)$$

where b_n is the clear width of the beam ($b-n\phi$), ϕ is the reinforcement diameter, and f_c the concrete compressive strength in MPa. The contribution of aggregate interlock, V_{ai} , can be determined in a simplified way (Yang, 2014) based on the fundamental analysis of aggregate interlock (Walraven, 1980, 1981) as:

$$V_{ai} = f_c^{0.56} s_{cr} b \frac{0.003}{w_b - 0.01 \text{ mm}} (-978\Delta^2 + 85\Delta - 0.27) \quad (6.12)$$

The critical shear displacement Δ_{cr} at shear failure replaces Δ in Eq. (6.12) and is empirically derived as:

$$\Delta_{cr} = \frac{25d}{30610\varphi} + 0.0022 \text{ mm} \leq 0.025 \text{ mm} \quad (6.13)$$

The crack width at the bottom of the cross section is:

$$w_b = \frac{M}{zA_s E_s} l_{cr,m} \quad (6.14)$$

with M the acting bending moment, and A_s the reinforcement area. If the height of the fully developed crack is s_{cr} , the crack spacing is:

$$l_{cr,m} = \frac{s_{cr}}{k_c} \quad (6.15)$$

with $k_c = 1.28$.

When $f_c > 65$ MPa, V_{ai} from Eq. (6.12) can be multiplied by the correction factor R_{ai} :

$$R_{ai} = 0.85 \sqrt{\left(\frac{7.2}{f_c - 40 \text{ MPa}} + 1\right)^2 - 1} + 0.34 \quad (6.16)$$

Once V_{CSDT} is determined for the cross section under consideration, the sectional analysis can be carried out to find the corresponding strain $\varepsilon_{c,bot}$ for which shear failure according to the CSDT is reached. This value is then limited to $\varepsilon_{c,bot,max} = 0.65\varepsilon_{c,bot}$ and the stop criterion from Eq. (6.7) can be determined. A similar stop criterion for the limiting crack width is derived, which is based on the assumption that shear capacity is lost when the aggregate interlock capacity becomes smaller than the inclined cracking load:

$$w_{ai} = w_d + 0.01 \text{ mm} \quad (6.17)$$

The value of w_d is determined as:

$$w_d = \frac{0.03f_c^{0.56} \frac{s_{cr}}{d} (978\Delta_{cr}^2 + 85\Delta_{cr} - 0.27)R_{ai}}{v_{RBK}} \quad (6.18)$$

with s_{cr} according to Eq. (6.10), Δ_{cr} from Eq. (6.13), R_{ai} from Eq. (6.16) and v_{RBK} the inclined cracking stress determined from the RBK (Rijkswaterstaat, 2013):

$$v_{RBK} = \max\left(1.13k_{slab} k \sqrt{\frac{f_c}{f_{ym}}}; 0.15k_{slab} k (100\rho_s f_c)^{1/3}\right) \quad (6.19)$$

with $k_{slab} = 1.2$ for slabs and 1.0 for other elements, and k the size effect factor:

$$k = 1 + \sqrt{\frac{200 \text{ mm}}{d}} \leq 2 \quad (6.20)$$

For cross sections that are not cracked in bending, the shear stop criterion for crack width becomes:

$$w_{max} \leq 0.4w_{ai} \quad (6.21)$$

For cross sections that are previously cracking in bending, the stop criterion is:

$$w_{max} \leq 0.75w_{ai} \quad (6.22)$$

Just as for the flexural stop criteria, crack widths smaller than 0.05 mm are neglected, a stop criterion for 25% reduction of stiffness in the load–displacement diagram is included, and qualitative stop criteria based on the longitudinal and transverse deformation profiles and the load–deflection diagram are added.

6.5.3 Comparison between measurements and stop criteria

In this section, the stop criteria from the German guideline ([Deutscher Ausschuss für Stahlbeton, 2000, 2020](#)) and the theoretically derived stop criteria for flexure ([Lantsoght et al., 2019c](#)) and shear ([Lantsoght et al., 2018c](#)) are analyzed ([Zarate Garnica and Lantsoght, 2019](#)).

For the bending moment test, the ratio of residual to maximum deformation (first flexural stop criterion of the German guideline) was 9.7% and for the shear test 9.7%. For both proof load tests, the first stop criterion is thus fulfilled. The residual deformation during the proof load test is measured at the moment when the base load level (10 kN) is still acting on the bridge. Unloading to 0 kN is not used during the bridge to keep all sensors activated.

The second stop criterion from the German guidelines is based on the strains in the concrete ([Eq. 6.1](#)). The maximum strain observed in the bending moment experiment is 240 $\mu\epsilon$ at LVDT 2. The value of ϵ_{c0} is determined from the linear finite element program. As a result, the maximum measured strain has to be smaller than $800 \mu\epsilon - 38 \mu\epsilon = 762 \mu\epsilon$, and this requirement is fulfilled. The maximum strain in the shear experiment was 224 $\mu\epsilon$ at LVDT 2, and the strain caused by the permanent loads is taken from the finite element model as 45 $\mu\epsilon$. The requirement now becomes that $224 \mu\epsilon$ has to be smaller than $800 \mu\epsilon - 45 \mu\epsilon = 755 \mu\epsilon$, and this requirement is fulfilled.

Since in the two-proof load test only existing cracks were monitored, only the stop criteria for existing cracks from the German guidelines need to be verified. An overview of these results is given in [Table 6.5](#) for the bending moment test and in [Table 6.6](#) for the shear test. For both cases, it can be seen that the studied crack widths are extremely small. However, since the German guidelines do not include a lower bound to crack widths that need to be considered, one would conclude that this stop criterion is violated for LVDT15 in the shear test. In reality, this stop criterion is not suitable for the case under consideration.

The next step is to compare the proposed stop criteria for flexure to the findings of the bending moment test and the proposed stop criteria for shear to the findings of the shear test. As mentioned previously, the maximum strain observed in the bending test was 240 $\mu\epsilon$. Using [Eq. \(6.2\)](#) the limiting strain is 842 $\mu\epsilon$ and the stop criterion is never exceeded. The measured crack widths (see [Table 6.5](#)) are all less than 0.05 mm, so that no structural cracking occurs. Using [Eq. \(6.4\)](#) the value of w_{stop} is

Table 6.5 Overview of maximum and residual crack width, and the limitation to the residual crack width during bending moment test.

| | Measured Δw (mm) | | $0.2 \times \Delta w$ (mm) |
|--------|--------------------------|---------------------|----------------------------|
| | During proof loading | After proof loading | |
| LVDT14 | -4×10^{-4} | -0.0014 | (no action) |
| LVDT15 | 0.0069 | -0.0013 | 0.00138 |
| LVDT16 | 0.0377 | 0.0032 | 0.00754 |

Table 6.6 Overview of maximum and residual crack width, and the limitation to the residual crack width during shear test.

| | Measured Δw (mm) | | $0.2 \times \Delta w$ (mm) |
|--------|--------------------------|---------------------|----------------------------|
| | During proof loading | After proof loading | |
| LVDT14 | 0.0163 | 0.0147 | 0.00326 |
| LVDT15 | 0.0248 | 0.0117 | 0.00496 |
| LVDT16 | 0.0183 | 0.0061 | 0.00366 |

0.17 mm, and this criterion is never exceeded. The criterion for residual crack width gives a limit of $w_{res,lim} = 0.007$ mm, which is never exceeded either, as the maximum residual crack width is neglected for being smaller than 0.05 mm. Indeed, the residual crack width stop criterion is not useful for small crack widths as occurring in this case study. The maximum stiffness reduction from the load–deflection diagram is 4%, which is smaller than the limit of 25% so that this stop criterion is fulfilled. In the load–deflection diagram, longitudinal deflection profile and transverse deflection profile, no changes in behavior are qualitatively observed, so that the qualitative stop criteria are also never exceeded. We can thus conclude that none of the proposed flexural stop criteria were exceeded in the bending moment test.

For the shear test, we can compare the maximum strain of $224 \mu\epsilon$ to the limit from Eq. (6.7), which can be calculated as $416 \mu\epsilon$ (Zarate Garnica and Lantsoght, 2019). The strain stop criterion for shear is thus never exceeded. The maximum crack width is less than 0.05 mm, so it is taken as 0 mm, and this value is smaller than the limit from Eq. (6.22), equal to 0.064 mm (Lantsoght, 2017) so that the crack width stop criterion is never exceeded. The maximum stiffness reduction is 10%, which is less than the limit of 25% and the stiffness stop criterion is never exceeded. In the load–deflection diagram, longitudinal deflection profile and transverse deflection profile, no changes in behavior are qualitatively observed, so that the qualitative stop criteria for this shear test are also never exceeded. We can thus conclude that none of the proposed shear stop criteria were exceeded in the shear test.

Since shear is a brittle failure mechanism, this failure needs to be avoided. Since shear stop criteria are still a topic of research, the acoustic emission measurements are used as well. These measurements give us more insight in the internal cracking occurring in the slab during the load test. The acoustic emission signals were followed closely to capture signs of increased cracking activity and instable crack development. In addition, the output of all sensors was closely followed to capture signs of changes to the structure and nonlinearity in addition to the previously discussed stop criteria. The effect of ASR damage on the shear capacity is unknown. On the one hand, the cracking caused by ASR reduces the uniaxial tensile strength, which is expected to reduce the shear capacity. On the other hand, the restraint of expansion in the direction of the reinforcement creates a prestressing effect on the cross section, which increases the shear capacity. As such, we took extra precautions to carry out this proof load test and closely followed the acoustic emissions, all sensor outputs, and the previously

discussed stop criteria. Based on the observations during the test and the analysis of the stop criteria discussed in the previous sections, we concluded that in the bending and shear test no signs of distress were observed under the applied loading. As such, we conclude that the bridge can carry the target proof load adequately.

6.5.4 Recommendations from load test

Both proof load tests on the viaduct Zijlweg were carried out successfully. It was shown experimentally that the viaduct can carry the loads prescribed by the code, using the load factors of the RBK Design load level with an additional 5% based on the resulting bending moment and shear in the critical section. This means that the structure fulfills the same requirements as a designed and newly built structure. The viaduct was monitored closely with a large number of sensors during the experiments, and no signs of distress were found. The final conclusion regarding the structural safety cannot be made and further research on the reliability-based substantiation of proof load testing is currently being performed (de Vries et al., 2021, 2022). This research will identify the correct method to determine the target proof load to fulfill the safety requirements from the code.

In 2002, a waterproofing layer was added on top of the slab to prevent durability problems resulting from further cracking caused by ASR. Providing waterproofing and preventing the ingress of moisture are a good solution to prevent further cracking and future durability problems, as moisture is required for the ASR gel to expand and cause cracking. Regular inspections and continued monitoring of the effects of ASR are necessary. Special attention should be paid to the space in the expansion joints, which has become small as a result of the longitudinal expansion of the slab caused by ASR. If this space would be fully taken up by the expanded superstructure, unintended bending moments and stresses caused by the restraint of further expansion can result.

6.6 Cost considerations

6.6.1 Sustainability-based cost for replacement

The literature indicates that there is a trend toward taking into account the cost of the structure over its entire life cycle in bridge engineering (Frangopol et al., 2016). Bridge engineering is changing from the previous concept of only considering the cost of design and construction, to a new paradigm of determining the cost of design, construction, inspection, maintenance, strengthening, demolition, and the salvage value (Kim and Frangopol, 2011). The so-called economic costs are those mentioned before. The cost to society and the environment must also be calculated for a complete sustainability-based cost analysis of a bridge (Gervasio et al., 2012; Beck et al., 2012). It is customary to rate buildings according to their sustainability using LEED and BREEAM certification concepts. Sustainability analyses for bridges, on the other hand, are still a subject of research (Yang et al., 2019; Wang et al., 2019; Liu et al., 2018; García-Segura et al., 2017; Frangopol et al., 2017; Frangopol and Soliman, 2016;

Sabatino et al., 2015; Dong et al., 2013, 2015; Hendy and Petty, 2012). The offer with the lowest initial cost is typically still the one that is chosen when a bridge project is put out to tender (Beck et al., 2012). Bridge authorities in some nations, like the United Kingdom, where the Sustainability Index for Bridges is developed (Hendy and Petty, 2012), are working to change the tide. The life cycle of a structure is typically divided into five stages (Beck et al., 2012):

1. the product stage,
2. the construction process,
3. the usage stage,
4. the end-of-life stage, and
5. the stage identified as “supplementary information beyond the building life cycle,” which contains benefit and loads beyond the system boundary.

When compared with buildings, the operation phase of bridges is much less significant. The construction stage and end-of-life stage become more significant in comparison to the other stages. The demolition procedures, material transportation, and final waste processing for reuse, recovery, and recycling during the end-of-life stage influence the total sustainability impact.

The economic, environmental, and social impact should be considered to evaluate the sustainability impact of proof load testing. The UK’s Sustainability Index for Bridges (Hendy and Petty, 2012) considers both the impact on climate change and the consumption of resources. The analysis will now be conducted under the assumption that the superstructure of the Zijlweg viaduct should be replaced, and the results will be compared to the results of the field test, which demonstrated that the viaduct satisfies the code requirements requirements. Due to the need to combine, weigh, and estimate several parameters, calculating the impact on sustainability is challenging. Not all parameters can be determined quantitatively. Additionally, integrating components from research fields that investigate the impact on society and the environment necessitates an understanding of ideas that are typically not covered in engineering education. Choosing how to weigh the various components of the complete evaluation presents an additional challenge. Before deciding on a specific repair or replacement plan, these various issues should be considered and examined.

6.6.2 Sustainability-based savings of replacement

The sustainability cost of replacing the superstructure of the viaduct Zijlweg (with its ASR affectation) is researched and contrasted with the cost of field testing to calculate the cost savings from the bridge’s proof load testing. It must be noted that a structure that passes a proof load test and is deemed adequate may still need to be replaced later on in its service life. Methods are currently being developed based on the annual reliability to identify the projected time in the future when the value of the reliability index drops below the value prescribed by the code (de Vries et al., 2022). This information can be used to schedule a future proof load test or plan another mitigation solution. Moreover, since the topic of the application of proof load testing to shear-

critical structures is still under development, it is expected that the cost of proof load testing will decrease significantly once standardization of the procedures is obtained.

The economic cost is calculated first. Based on the Dutch construction cost for slab bridges, which ranges between 800 and 1000 €/m², the expected cost can be estimated. The viaduct Zijlweg has four spans: two end spans measuring 10.32 m and two middle spans measuring 14.71 m. Its width is 6.6 m, and its total area is 330.4 m². Thus, assuming that the geometry is left unchanged, the economic cost of replacing the superstructure would range from 264,300 to 330,400 €. It would be more expensive to build a bridge with more than one lane of traffic, and there is also the risk that the substructure already in place won't be strong enough to support the extra weight, which would require a strengthening of the substructure as well.

The Carbon Calculator for Construction Activities is used to evaluate the environmental impact (Environment Agency, 2016). For this purpose, we determine the total volume of concrete first. Since the slab's thickness can range from 550 to 850 mm, the average thickness of 700 mm is used for these calculations to get an estimate of the total volume. Assuming that the replacement bridge will have a design that is very similar to the existing bridge, multiplying this number by the area of 330.4 m² results in a volume of 232 m³ of concrete. The amount of reinforcement steel needs to be calculated after that. A value of approximately 28 tons of steel is obtained by assuming that there is 120 kg of steel in every 1 m³ of concrete. The reinforcement steel's carbon footprint is 41 tons of CO₂ if there is a 75-km distance between the producer and the construction site. The estimated carbon footprint of the concrete is 67 ton CO₂ for 232 m³ of XC4-exposed concrete and a 20-km distance between the plant and the construction site. An additional footprint of 15 tons of CO₂ is created by the transportation of personnel with fewer than eight people on site for 48 weeks. The overall resulting footprint is 109 tons of CO₂. Fig. 6.29 shows the breakdown of the various contributions considered. Some components are not taken into account in this calculation: (1) the life cycle conversion factors for waste disposal, (2) the emissions from plant and equipment, (3) the fuel consumption on site, and (4) the distance over which this fuel is transported. It is difficult to predict the choice of fuel a priori as this choice depends on the contractor. It is necessary to divide this fuel consumption between the on-site plant, equipment, and site accommodations. A diesel generator, for instance, could be used to run both the site offices and a mobile plant. For the analyzed project, which is relatively small, only electricity for the temporary site offices is deemed necessary. It becomes possible to calculate this additional carbon footprint contribution from using fuel on-site as well as from the amount of water used on the job site.

The breakdown in Fig. 6.29 is based on the assumption of using Portland cement. It's interesting to investigate the impact of using various types of cement because concrete makes up the largest portion of the superstructure's carbon footprint. The types of cement that are examined here are: Portland cement (with 6% limestone), Portland fly ash cement (28% fly ash), Portland slag cement (35% ggbs), blastfurnace slag cement (80% ggbs), and pozzolanic cement (with fly ash and 45% ggbs). Table 6.7 summarizes the findings of this analysis and the resulting decrease in CO₂ emissions. The assumption that 14% of the weight of the total concrete is the weight of cement lies at the basis of these results. A weight of 556.8 ton of concrete, or 78 tons of cement, is

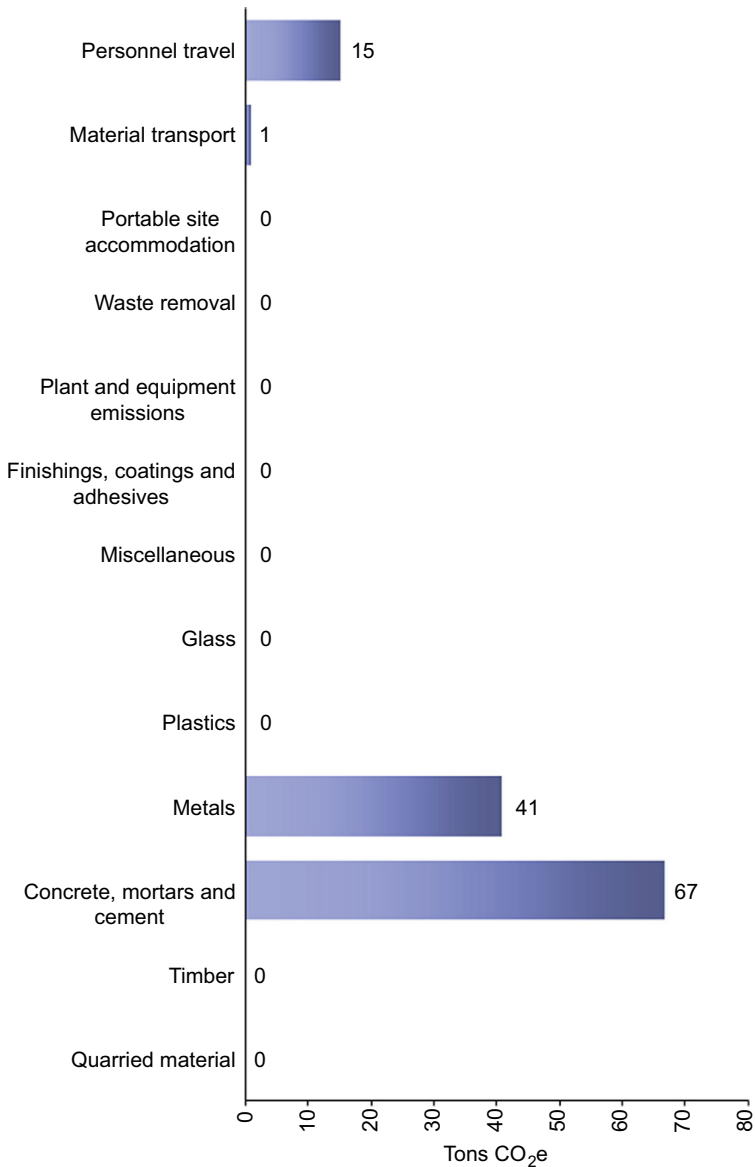


Figure 6.29 Breakdown of contributions of construction materials and transportation on total carbon footprint of replacement of superstructure.

obtained for 232 m³ of concrete, assuming a density of 2.4 ton/m³. The effect of improved concrete mixtures with reduced amounts of cement, or alkali-activated concrete mixes without Portland cement (Qian et al., 2022), is not considered here. As shown in Table 6.7, using blastfurnace slag cement (which contains 80% ggbs) results

Table 6.7 Effect of choice of type of cement on total carbon footprint of replacement of superstructure.

| Type of cement | CO ₂ emission (tCO ₂ eq/ton of cement) | Total CO ₂ cement (tCO ₂ eq) | Total CO ₂ superstructure (tCO ₂ eq) | Saving (%) |
|-------------------------|--|--|--|------------|
| Portland cement | 0.88 | 68.60 | 110.2 | - |
| Portland fly ash cement | 0.67 | 52.23 | 93.83 | 14.9 |
| Portland slag cement | 0.62 | 48.33 | 89.93 | 18.4 |
| Blastfurnace slag | 0.23 | 17.93 | 59.53 | 46.0 |
| Pozzolanic cement | 0.51 | 39.76 | 81.36 | 26.2 |

in significant carbon footprint reductions: 46% of the carbon emissions are avoided compared with using Portland cement (which contains 6% limestone). Due to its availability, blastfurnace slag is the cementitious material of choice in the Netherlands. This standard option has a significant, beneficial impact on the environment.

Last but not least, the social dimension is influenced by a wide range of factors, including visual impact, delays in travel time, employment opportunities, and more (Zinke et al., 2012). Currently, costs associated with driver delays are used to calculate the social impact most frequently, as these can be quantified. As a result of the construction site's traffic obstruction and the need for drivers to take an alternate route, additional traffic congestion is created, which adds to the costs associated with driver delays. The location of the structure is a major factor in determining these costs. As it has been demonstrated that for bridges in densely populated areas, the driver delay costs can be as much as nine times higher than the direct economic costs (Zinke et al., 2012), the social costs should not be ignored. Less than 250,000 vehicles use the Zijlweg viaduct each year. The total driver delay cost for a year of demolition and superstructure replacement can be estimated at 833,000 €, which is 2.8 times greater than the direct economic cost, assuming a driver delay cost of 10 €/vehicle/hour and a 20-minute delay caused by rerouting to the next bridge. This preliminary estimate demonstrates that the social impact of driver delays is significant, even for a bridge that is only used by local traffic.

Similar calculations can be made for the sustainability cost and benefits of using a proof load test for the assessment of the viaduct Zijlweg. Again, it must be stressed that further standardization and implementation of proof load testing will reduce the execution costs, as for the viaduct Zijlweg the instrumentation was redundant, and budget for research was included. Moreover, the practice of proof load testing of shear-critical structures is still in the stage of research. With standardized stop criteria for shear, the cost of instrumentation will reduce.

The economic cost entails the cost of applying the load, the cost of material research, the cost of scaffolding and site preparations, as well as a research budget on the subject of proof load testing in relation to this pilot. As a result, the economic cost, which is approximately 80,000 €, can be decreased after the procedures have

been standardized. It should be noted that this cost includes a budget for research to achieve standardization and optimization, whereas no research budget is needed for the option of replacing the superstructure. Currently, only the transportation of people to the construction site has an environmental impact, which is approximately 0.3 tCO₂. The driver delays are calculated for the social cost under the assumptions of a price of 10€/vehicle/hour and a detour of 20 minutes. In total, 3425 vehicles were impacted by the bridge's 5-day closure, causing 11,415 € in driver delays. Due to the testing taking place over the summer break, this value is probably even lower.

This sustainability cost calculation highlights the significant economic, environmental, and social cost savings that come from using proof load testing to more accurately assess reinforced concrete slab bridges. The average cost of replacing the ASR-affected superstructure would be 297,000 €, and using blast furnace slag cement with a ggbs content of 80% would result in carbon emissions of at least 60 tCO₂. Driver delays would also add significantly to the cost. On the other hand, the proof load test demonstrated that the ASR-affected superstructure satisfies the code requirements and can carry the prescribed loads without showing signs of distress. This finding avoids replacement costs for the superstructure. The remaining costs of the service life of the existing structure are as determined in the maintenance plan, and these have been budgeted for. A field tests (including a research budget) currently costs about 27% of a replacement, results in negligible CO₂ emissions, and leads to only 1% of the driver delay costs of a replacement scheme. Finalization of the research will lead to standardization and optimization, so that a cost of 5%–10% of the replacement cost (for the economic cost) is hoped to be achieved in the future. As a result, it is clear that field testing offers significant cost savings, and that the benefits to the environment and social cost savings outweigh the economic costs by a wide margin. Thus, the choice of field testing becomes even more appealing when taking into account a full sustainability analysis than when only considering economic costs.

One last observation is that the significant savings realized through proof load testing are only valid when the proof load test is successful, that is, when the tested structure can carry the applied target proof loads and replacement is not required. Determining which bridge structures are strong candidates for proof load testing is crucial for this reason. Bridges without plans, bridges anticipated to have significant redistribution capacity beyond codified calculation methods, and bridges where the impact of material degradation on structural capacity is unknown are particularly interesting structures in this regard. Guidelines on how to select good candidate structures for proof load testing have been published recently (Alampalli et al., 2019), and Dutch guidelines for proof load testing of shear-critical structures are currently being developed.

6.7 Future trends

Current research on the topic of field assessment through load testing focuses on the reliability aspects of the determined target proof load (de Vries et al., 2022), and on determining stop criteria for shear (Zarate Garnica and Lantsoght, 2020). Currently, several countries (Germany, USA, Denmark, the Netherlands) are working toward the

development of or the updating of the guidelines for field testing of bridges, with several improvements published over the past years (Deutscher Ausschuss für Stahlbeton, 2020; Alampalli et al., 2019; Lantsoght et al., 2017d). Load testing is more and more important for existing structures, as it is an excellent method to assess the structure in its real conditions. As more of the existing bridges are aging and the traffic loads and volumes are increasing, more accurate methods for the assessment of existing bridges are necessary. Similarly, as many countries face this challenge, international collaboration is key (Lantsoght, 2022). This objective is being addressed by the formation in 2021 of an international committee of IABMAS (the International Association for Bridge Maintenance and Safety) on Bridge Load Testing.

Researchers in the Netherlands are working on creating guidelines for the proof load testing of existing concrete bridges for the industry. To achieve this goal, research on stop criteria for shear is necessary and currently underway. Additionally, it is critical to understand how the practice of proof load testing can fit within the probability-based design and assessment codes through the probabilistic substantiation of proof load testing, which is a second topic of researcher. Finally, quicker ways to figure out the target proof load and advice for the minimum amount of sensors needed must be created. These steps are essential to the development of a quick, low-cost proof load testing technique that will allow the industry to assess existing bridges with relative ease.

6.8 Summary and conclusions

The assessment of existing bridges is becoming more crucial due to the aging of the existing bridge stock. The feasibility of proof load testing as a low-cost approach for a direct field evaluation of an existing bridge is a topic of research. Cracking brought on by ASR damage raised questions about the shear capacity of the viaduct Zijlweg, so this viaduct was chosen as a pilot project.

Gaining more experience in the method of proof load testing was the primary objective of the viaduct Zijlweg proof load test. To monitor the structural response during the proof load tests and to assess the usefulness of both the existing stop criteria from the German guideline (which are theoretically only valid for flexure) and proposed stop criteria for flexure and shear derived from theoretical considerations, a comprehensive sensor plan was developed. The analysis of the stop criteria showed that the crack width stop criteria from the German guideline are not suitable for proof load testing of bridges. The proposed stop criteria for flexure and shear were never exceeded, which indicates that these criteria are not overly conservative, as no signs of distress were observed during the test based on a detailed analysis of the sensor output, the acoustic emission measurements, and the evaluation of the overall behavior of the bridge.

The proof load testing of the Zijlweg viaduct's second objective was to demonstrate experimentally that the structure can support the code-prescribed loads without showing signs of structural distress. While a probabilistic substantiation of the target proof load is the topic of current research, we can conclude that with our current knowledge the bridge has shown to be able to carry the code-prescribed factored live loads.

The cost savings from a sustainability standpoint were calculated based on the outcome that the proof load test was successful. The biggest cost savings relate to the environmental cost (avoiding at least 60 tCO₂eq associated with the replacement of the superstructure) and the indirect economic cost related to driver delays (a difference of 821,585 € between a superstructure replacement and a proof load test). As such, from a sustainability perspective and in the light of eco-efficiency, proof load testing can be an excellent solution for the assessment of existing reinforced concrete bridges where analytical or numerical methods are insufficient or large uncertainties prevent us from using refined analytical or numerical analyses.

Acknowledgments

I'd like to express my gratitude and sincere appreciation to the Dutch Ministry of Infrastructure and the Environment (Rijkswaterstaat) and the Province of Noord Brabant for financing this pilot-proof load test. I'd also like to thank Rutger Koekkoek from Delft University of Technology for all his contributions to the preparation of the test, the finite element modeling, the planning, the on-site work, and the evaluation of the experiment. Thanks to Prof. Dick Hordijk from Delft University of Technology for the coordination of the project and the photographs from the visual inspection he did. I'd also like to acknowledge Dr. Ane de Boer from Rijkswaterstaat for all his input and the fruitful discussions on the proof load test, and Dr. Sonja Fennis and Marius Naaktgeboren from Rijkswaterstaat for the input and fruitful discussions in the light of the ongoing research projects related to proof load testing.

Credit also goes to former M.Sc. student Werner Vos of Delft University of Technology, who analyzed the data of the ASR-monitoring and patiently drew the map of cracks. The contributions and help of our colleagues Albert Bosman, Dr. Cor van der Veen, and Dr. Yuguang Yang, and of student Arthur Ennouri from Delft University of Technology during planning, execution, and analysis of this proof load test have been of great value and help, and are gratefully acknowledged. I'm also thankful for the fruitful discussions with Frank Linthorst and Danny den Boef of Witteveen + Bos, responsible for the logistics and safety, and with Otto Illing and the late Chris Huissen of Mammoet, responsible for applying the load.

Many thanks to doctoral candidates Gabriela Zarate Garnica and Rein de Vries from Delft University of Technology for their research on proof load testing, and Albert Bosman and Jakub Pawlowicz for the work in the laboratory on the slab experiments to determine shear stop criteria. I would also like to thank Sebastian Castellanos-Toro from Universidad del Valle in Cali, Colombia for the research on diagnostic load testing of planless prestressed bridges. In addition, I would like to thank all MSc thesis students from Delft University of Technology and BSc thesis students from Universidad San Francisco de Quito who worked on the topic of load testing over the past years.

References

- ACI Committee 437, 2013. Code Requirements for Load Testing of Existing Concrete Structures (ACI 437.2M-13) and Commentary Farmington Hills, MA.
- Ahmed, T., Burley, E., Rigden, S., 1998. The static and fatigue strength of reinforced concrete beams affected by alkali-silica reaction. *ACI Mater. J.* 95, 376–388.

- Ahmed, T., Burley, E., Rigden, S., 1999. Effect of alkali-silica reaction on tensile bond strength of reinforcement in concrete tested under static and fatigue loading. *ACI Mater. J.* 96, 419–428.
- Alampalli, S., Frangopol, D.M., Grimson, J., Halling, M.W., Kosnik, D.E., Lantsoght, E.O.L., et al., 2021. Bridge load testing: state-of-the-practice. *J. Bridge Eng.* 26, 03120002.
- Alampalli, S., Frangopol, D.M., Grimson, J., Kosnik, D., Halling, M., Lantsoght, E.O.L., et al., 2019. Primer on Bridge Load Testing. Transportation Research Board E-circular 257.
- Albraheemi, M.J.A., Davids, W.G., Schanck, A., Tomlinson, S., 2019. Evaluation and rating of older non-composite steel girder bridges using field live load testing and nonlinear finite element analysis. *Bridge Struct.* 15, 27–41.
- Bagge, N., Sas, G., Nilimaa, J., Blanksvard, T., Elfgrén, L., Tu, Y., et al., 2015. Loading to failure of a 55 year old prestressed concrete bridge. IABSE Workshop, Helsinki, Finland.
- ASCE-SEI-AASHTO Ad-Hoc Group On Bridge Inspection Rating Rehabilitation And Replacement, 2009. White paper on bridge inspection and rating. *J. Bridge Eng.* 14, 1–5.
- Barker, M.G., 2001. Quantifying field-test behavior for rating steel girder bridges. *J. Bridge Eng.* 6, 254–261.
- Baumann, T., Rusch, H., 1970. Versuche zum Studium der Verdübelungswirkung der Biegezugbewehrung eines Stahlbetonbalkens. *DAfStB. Heft 210*, 87–pp.
- Beck, T., Fischer, M., Pfaffinger, M., 2012. Life cycle assessment for representative steel and composite bridges. In: Biondini, F., Frangopol, D.M. (Eds.), *Proceedings of the Sixth International Conference on Bridge Maintenance, Safety and Management*. Taylor & Francis Group, Stresa, Lake Maggiore, Italy.
- Bertola, N.J., Henriques, G., Schumacher, T., Brühwiler, E., 2022. Engineering of existing structures: the need and place for non-destructive evaluation. NDT-CE 2022-The International Symposium on Nondestructive Testing in Civil Engineering (NDT-CE) 2022. Zurich, Switzerland, August 16-18, 2022. 10 pp.
- Bonifaz, J., Zaruma, S., Robalino, A., Sanchez, T.A., 2018. Bridge diagnostic load testing in ecuador – case studies. IALCCE 2018, Ghent, Belgium.
- Borges, E.A.A., Lantsoght, E.O.L., Castellanos-Toro, S., Casas, J.M., 2021. Modeling and analysis of a prestressed girder bridge prior to diagnostic load testing. *ACI Avances en Ciencias e Ingenierías* 13.
- Catbas, F.N., Kijewski-Correa, T.L., Aktan, A.E., 2013. *Structural Identification of Constructed Systems: Approaches, Methods, and Technologies for Effective Practice of St-Id*. Structural Engineering Institute. Committee on Structural Identification of Constructed Systems.
- CEN, 2002. Eurocode – Basis of structural design, NEN-EN 1990:2002 Brussels, Belgium: Comité Européen de Normalisation.
- CEN, 2003. Eurocode 1: Actions on structures – Part 2: Traffic loads on bridges, NEN-EN 1991–2:2003. Brussels, Belgium: Comité Européen de Normalisation.
- CEN, 2011. Eurocode 2: Design of concrete structures – Concrete bridges – Design and detailing rules. NEN-EN 1992-2 + C1:2011. Brussels, Belgium: Comité Européen de Normalisation.
- Chen, X., 2019. Critical proof load for proof load testing of concrete bridges based on scripted FEM analysis. IALCCE 2018. In: Taerwe (Eds.), *Life-Cycle Analysis and Assessment in Civil Engineering: Towards an Integrated Vision - Proceedings of the 6th International Symposium on Life-Cycle Civil Engineering*, IALCCE, CRC Press/Balkema - Taylor & Francis Group, pp. 99–105.

- Christensen, C.O., Schmidt, J.W., Halding, P.S., Kapoor, M., Goltermann, P., 2021. Digital image correlation for evaluation of cracks in reinforced concrete bridge slabs. *Infrastructures* 6.
- Christensen, C.O., Zhang, F., Garnica, G.Z., Lantsoght, E.O.L., Goltermann, P., Schmidt, J. W., 2022. Identification of stop criteria for large-scale laboratory slab tests using digital image correlation and acoustic emission. *Infrastructures* 7, 36.
- Code Committee 351001, 2011a. Assessment of structural safety of an existing structure at repair or unfit for use – Basic Requirements, NEN 8700:2011 (in Dutch), Delft, The Netherlands, Civil center for the execution of research and standard, Dutch Normalisation Institute.
- Code Committee 351001, 2011b. Eurocode 1 – Actions on structures – Part 2: Traffic loads on bridges, EN 1991-2/NA:2011. Delft, The Netherlands: Civil engineering center for research and regulation, Dutch Normalization Institute.
- Commander, B., 2019. Evolution of bridge diagnostic load testing in the USA. *Front. Built Environ.* 5.
- Cope, R.J., 1985. Flexural shear failure of reinforced-concrete slab bridges. *Proc. Inst. Civ. Eng. Part. 2-Res. Theory* 79, 559–583.
- Cope, R.J., Rao, P.V., Edwards, K.R., 1983. Shear in Skew Reinforced Concrete Slab Bridges – Analytical and Experimental Studies – A report to the Department of Transport. University of Liverpool, Liverpool, UK.
- Den Uijl, J.A., Kaptijn, N., 2004. Structural consequences of ASR: an example on shear capacity. *Heron* 47, 1–13.
- Deutscher Ausschuss Für Stahlbeton, 2000. DAFStb-Guideline: Load Tests on Concrete Structures (in German) (DAFStb-Richtlinie: Belastungsversuche an Betonbauwerken). Deutscher Ausschuss für Stahlbeton, Berlin, Germany, p. 8.
- Deutscher Ausschuss Für Stahlbeton, 2020. DAFStb-Richtlinie: Belastungsversuche an Betonbauwerken. Deutscher Ausschuss für Stahlbeton.
- De Vries, R., Lantsoght, E.O.L., Steenbergen, R.D.J.M., 2021. Case Study Proof Loading in an Annual Reliability Framework. Delft University of Technology, Delft, the Netherlands.
- De Vries, R., Lantsoght, E.O.L., Steenbergen, R.D.J.M., Fennis, S.A.A.M., 2022. Reliability assessment of existing reinforced concrete bridges and viaducts through proof load testing. IABMAS 2022 Barcelona, Spain.
- Dong, Y., Frangopol, D.M., Sabatino, S., 2015. Optimizing bridge network retrofit planning based on cost-benefit evaluation and multi-attribute utility associated with sustainability. *Earthq. Spectra* 31, 2255–2280.
- Dong, Y., Frangopol, D.M., Saydam, D., 2013. Time-variant sustainability assessment of seismically vulnerable bridges subjected to multiple hazards. *Earthq. Eng. & Struct. Dyn.* 42, 1451–1467.
- Ensink, S.W.H., Van Der Veen, C., Hendriks, M.A.N., 2019. Non-Linear Analysis of Prestressed Concrete T-beams. SEMC 2019, Cape Town, South Africa.
- Ensink, S.W.H., Van Der Veen, C., Hordijk, D.A., Lantsoght, E.O.L., Van Der Ham, H., De Boer, A., 2018. Full-size field test of prestressed concrete T-beam bridge. European Bridge Conference. Edinburgh, Scotland.
- Environment Agency. 2016. Carbon calculator for construction activities [Online]. Available from: <https://www.ice.org.uk/disciplines-and-resources/best-practice/environment-agency-carbon-calculator-tool>.
- Faber, M.H., Val, D.V., Stewart, M.G., 2000. Proof load testing for bridge assessment and upgrading. *Eng. Struct.* 22, 1677–1689.

- Frangopol, D.M., Dong, Y., Sabatino, S., 2017. Bridge life-cycle performance and cost: analysis, prediction, optimisation and decision-making. *Struct. Infrastruct. Eng.* 13, 1239–1257.
- Frangopol, D.M., Sabatino, S., Dong, Y., 2016. Bridge life-cycle performance and cost: analysis, prediction, optimization and decision making. In: Bittencourt, F., Beck, A. (Eds.), *Maintenance, Monitoring, Safety, Risk and Resilience of Bridges and Bridge Networks*. Routledge, Foz do Iguacu, Brazil.
- Frangopol, D.M., Soliman, M., 2016. Life-cycle of structural systems: recent achievements and future directions. *Struct. Infrastruct. Eng.* 12, 1–20.
- Frangopol, D.M., Yang, D.Y., Lantsoght, E.O.L., Steenbergen, R.D.J.M., 2019. Chapter 9: Reliability-based analysis and life-cycle management of load tests. In: Lantsoght, E.O.L. (Ed.), *Load Testing of Bridges: Proof Load Testing and the Future of Load Testing*. Structures and Infrastructures. Taylor & Francis, Series Editor: D.M. Frangopol.
- García-Segura, T., Yepes, V., Frangopol, D.M., Yang, D.Y., 2017. Lifetime reliability-based optimization of post-tensioned box-girder bridges. *Eng. Struct.* 145, 381–391.
- Gervasio, H., Silva, L.S.D., Perdigao, V., Barros, P., Orcesi, A., Nielsen, K., 2012. Life Cycle analysis of highway composite bridges. In: Biondini, F., Frangopol, D.M. (Eds.), *Proceedings of the Sixth International Conference on Bridge Maintenance, Safety and Management*. Taylor & Francis Group, Stresa, Lake Maggiore, Italy.
- Gielen, C., Kolkman, M., Veldhuizen, A.C., 2008. Inspection report object 44G-113-01: bridge over highway – Zijlweg (in Dutch). 26 pp.
- Haddad, R.H., Shannag, M.J., Al-Hambouth, M.T., 2008. Repair of reinforced concrete beams damaged by alkali-silica reaction. *Acı Struct. J.* 105, 145–153.
- Halding, P.S., Schmidt, J.W., Christensen, C.O., 2018. DIC-monitoring of full-scale concrete bridge using high-resolution Wideangle lens camera. In: *Maintenance, Safety, Risk, Management and Life-Cycle Performance of Bridges – Proceedings of the 9th International Conference on Bridge Maintenance, Safety and Management, IABMAS 2018*, 1492–1499.
- Halicka, A., Hordijk, D.A., Lantsoght, E.O.L., 2018. Rating of concrete road bridges with proof loads. *ACI SP. 323 Evaluation Concr. Bridge Behav. Load. Test. – Int. Perspect.*, 16.
- Haritos, N., Hira, A., Mendis, P., Heywood, R., Giufre, A., 2000. Load testing to collapse limit state of Barr Creek Bridge. In: *Fifth International Bridge Engineering Conference*, Vols. 1 and 2: Bridges, Other Structures, and Hydraulics and Hydrology.
- Hendy, C., Petty, R., 2012. Quantification of sustainability principles in bridge projects. In: Biondini, F., Frangopol, D.M. (Eds.), *Proceedings of the Sixth International Conference on Bridge Maintenance, Safety and Management*. Taylor & Francis Group, Stresa, Lake Maggiore, Italy.
- Hernandez, E.S., Myers, J.J., 2018. Diagnostic test for load rating of a prestressed SCC bridge. *ACI Spec. Publ.* 323.
- Jauregui, D.V., Weldon, B.D., Aguilar, C.V., 2019. Chapter 3: Load rating of prestressed concrete bridges without design plans by non-destructive field testing. In: Lantsoght, E. O.L. (Ed.), *Load Testing of Bridges: Proof Load Testing and the Future of Load Testing*. Structures and Infrastructures. Taylor & Francis, D.M. Frangopol.
- Kim, S., Frangopol, D.M., 2011. Cost-effective lifetime structural health monitoring based on availability. *J. Struct. Eng.* 137, 22–33.
- KNMI. 2015. Uurgegevens van het weer in Nederland [Online]. Available from: http://www.knmi.nl/klimatologie/uurgegevens/datafiles/350/uurgeg_350_2011-2020.zip. (accessed 26.06.15).
- Koekkoek, R.T., Lantsoght, E.O.L., Hordijk, D.A., 2015. Proof Loading of the ASR-Affected Viaduct Zijlweg Over Highway A59. Delft University of Technology, Delft, The Netherlands.

- Koekkoek, R., Lantsoght, E., Yang, Y., Boer, A.D., Hordijk, D., 2016. Defining loading criteria for proof loading of existing reinforced concrete bridges. fib symposium 2016: Performance-based approaches for concrete structures, Cape Town, South Africa.
- Koenders Instruments, 2015. Zijlweg monitoring system (in Dutch).
- Lantsoght, E., 2017. Development of a Stop Criterion for Shear Based on Aggregate Interlock. Delft University of Technology.
- Lantsoght, E.O.L., Bonifaz, J., Sanchez, T.A., Harris, D.K., 2019a. Chapter 8: Methodology for diagnostic load testing. In: Lantsoght, E.O.L. (Ed.), *Load Testing of Bridges: Current practice and Diagnostic Load Testing*. Structures and Infrastructures. Taylor & Francis, D.M. Frangopol.
- Lantsoght, E.O.L., De Boer, A., Van Der Veen, C., Hordijk, D.A., 2019b. Optimizing finite element models for concrete bridge assessment with proof load testing. *Front. Built Environ.* 5.
- Lantsoght, E.O.L., De Boer, A., Van Der Veen, C., Walraven, J.C., 2013a. Peak shear stress distribution in finite element models of concrete slabs. In: Zingoni, A. (Ed.), *Research and Applications in Structural Engineering, Mechanics and Computation*. Taylor and Francis, Cape Town, South Africa.
- Lantsoght, E.O.L., Koekkoek, R.T., Hordijk, D.A., Boer, A., D.E., 2017b. Towards standardization of proof load testing: pilot test on viaduct Zijlweg. *Struct. Infrastruct Eng.* 16.
- Lantsoght, E., Okumus, P., 2018a. SP-323: Evaluation of Concrete Bridge Behavior through Load Testing – International Perspectives. *ACI Symposium Publication*, p. 323.
- Lantsoght, E.O.L., Van Der Veen, C., De Boer, A., Hordijk, D.A., 2016b. Probabilistic prediction of the failure mode of the Ruytenschildt Bridge. *Eng. Struct.* 127, 549–558.
- Lantsoght, E.O.L., Van Der Veen, C., De Boer, A., Hordijk, D.A., 2017c. Collapse test and moment capacity of the Ruytenschildt Reinforced Concrete Slab Bridge. *Struct. Infrastruct Eng.* 13, 1130–1145.
- Lantsoght, E.O., van der Veen, C., de Boer, A., Hordijk, D.A., 2018b. Assessment of slab bridges through proof loading in the Netherlands. *ACI Special Publication*, 323, 1-1.
- Lantsoght, E.O.L., Van Der Veen, C., De Boer, A., Walraven, J., 2014. Influence of width on shear capacity of reinforced concrete members. *ACI Struct. J.* 111, 1441–1450.
- Lantsoght, E.O.L., Van Der Veen, C., De Boer, A., Walraven, J., 2015a. One-way slabs subjected to combination of loads failing in shear. *ACI Struct. J.* 112, 417–426.
- Lantsoght, E.O.L., Van Der Veen, C., De Boer, A., Walraven, J.C., 2013b. Recommendations for the shear assessment of reinforced concrete slab bridges from experiments. *Struct. Eng. Int.* 23, 418–426.
- Lantsoght, E.O.L., Van Der Veen, C., De Boer, A., Walraven, J.C., 2015b. Proposal for the extension of the Eurocode shear formula for one-way slabs under concentrated loads. *Eng. Struct.* 95, 16–24.
- Lantsoght, E., Van Der Veen, C., Hordijk, D., De Boer, A., 2017a. Recommendations for proof load testing of reinforced concrete slab bridges. 39th IABSE Symposium – Engineering the Future, Vancouver, Canada.
- Lantsoght, E.O.L., Van Der Veen, C., Hordijk, D., 2017d. State-of-the Art Rapport Proefbelasten: Aanbevelingen en Discussiepunten. Delft University of Technology.
- Lantsoght, E.O.L., Van Der Veen, C., Hordijk, D.A., 2018c. Proposed stop criteria for proof load testing of concrete bridges and verification. IALCCE 2018, Ghent, Belgium.
- Lantsoght, E.O.L., Van Der Veen, C., Walraven, J., De Boer, A., 2015c. Experimental investigation on shear capacity of reinforced concrete slabs with plain bars and slabs on elastomeric bearings. *Eng. Struct.* 103, 1–14.

- Lantsoght, E.O.L., Van Der Veen, C., Walraven, J.C., 2013c. Shear in one-way slabs under a concentrated load close to the support. *ACI Struct. J.* 110, 275–284.
- Lantsoght, E. O. L., Yang, Y., Tersteeg, R. H. D., van der Veen, C., & De Boer, A. (2016, November). Development of stop criteria for proof loading. In *Life-Cycle of Engineering Systems: Emphasis on Sustainable Civil Infrastructure*, Proceedings of the 5th International Symposium on Life-Cycle Engineering, IALCCE.
- Lantsoght, E., Yang, Y., Van Der Veen, C., De Boer, A., Hordijk, D., 2016a. Ruytenschildt Bridge: field and laboratory testing. *Eng. Struct.* 128, 111–123.
- Lantsoght, E.O., 2022. Assessment of existing concrete bridges by load testing. In: *Bridge Safety, Maintenance, Management, Life-Cycle, Resilience and Sustainability: Proceedings of the Eleventh International Conference on Bridge Maintenance, Safety and Management (IABMAS 2022)*, Barcelona, Spain, July 11–15, 2022. CRC Press, 46.
- Lantsoght, E.O.L. (Ed.), 2019a. *Load Testing of Bridges: Current Practice and Diagnostic Load Testing*. CRC Press, Boca Raton, FL.
- Lantsoght, E.O.L. (Ed.), 2019b. *Load Testing of bridges: Proof Load Testing and the Future of Load Testing*. CRC Press, Boca Raton, FL.
- Lantsoght, E.O.L., Yang, Y., Van Der Veen, C., De Boer, A., Hordijk, D.A., 2017e. Determination of loading protocol and stop criteria for proof loading with beam tests. *fib symposium 2017*. Maastricht, the Netherlands.
- Lantsoght, E. O., Yang, Y., van der Veen, C., Hordijk, D. A., & De Boer, A. (2018). Stop criteria for proof load tests verified with field and laboratory testing of the Ruytenschildt Bridge. In *IABSE Conference 2018—Engineering the Past, to Meet the Needs of the Future and laboratory testing of the Ruytenschildt Bridge*. IABSE 2018, Copenhagen, Denmark.
- Lantsoght, E.O.L., Yang, Y., Van Der Veen, C., Hordijk, D.A., De Boer, A., 2019c. Stop criteria for flexure for proof load testing of reinforced concrete structures. *Front. Built Environ.* 5.
- Lin, T.S., Nowak, A.S., 1984. Proof loading and structural reliability. *Reliab. Eng.* 8, 85–100.
- Liu, L., Frangopol, D.M., Mondoro, A., Yang, D.Y., 2018. Sustainability-informed bridge ranking under scour based on transportation network performance and multiattribute utility. *J. Bridge Eng.* 23, 04018082.
- Liu, Y., Lu, D., Fan, X., 2014. Reliability updating and prediction of bridge structures based on proof loads and monitored data. *Constr. Build. Mater.* 66, 795–804.
- Marx, S., Grünberg, J., Schacht, G., 2019. Methods to evaluate test results based on small sample sizes. *Civ. Eng. Des.* 1, 74–84.
- Matta, F., Bastianini, F., Galati, N., Casadei, P., Nanni, A., 2008. Distributed strain measurement in steel bridge with fiber optic sensors: validation through diagnostic load test. *J. Perform. Constr. Facil.* 22, 264–273.
- Ministerio De Fomento, Direccion General De Carreteras, 1999. *Recomendaciones para la realizacion de pruebas de carga de recepcion en puentes de carretera*. Madrid. Spain 22.
- Morsch, E., 1922. *Der Eisenbetonbau: Seine Theorie Und Anwendung*. Verlag Von Konrad Wittwer, Stuttgart.
- Nilimaa, J., Blanksvärd, T., Taljsten, B., 2015. Assessment of concrete double-trough bridges. *J. Civ. Struct. Health Monit.* 2015, 29–36.
- Olaszek, P., Lagoda, M., Casas, J.R., 2014. Diagnostic load testing and assessment of existing bridges: examples of application. *Struct. Infrastruct Eng.* 10, 834–842.
- Paredes, J.E., Lantsoght, E.O.L., 2018. Nonlinear finite element analysis of beam experiments for stop criteria. *IALCCE 2018*, Ghent, Belgium. *Life Cycle Analysis and*

- Assessment in Civil Engineering: Towards an Integrated Vision: Proceedings of the Sixth International Symposium on Life-Cycle Civil Engineering (IALCCE 2018), 28-31 October 2018, Ghent, Belgium* (Vol. 5, p. 115). CRC Press.
- Projectteam RWS/TNO Bouw. (1997). Veiligheidsbeoordeling voor bestaande constructies: Gewapend betonnen kunstwerken. 102 pp Safety evaluation existing structures: Reinforced concrete bridges (in Dutch).
- Provincie Noord Brabant, 1965. Viadukt in de Zijlweg. 1965.
- Puurula, A.M., Enochsson, O., Sas, G., Blanksvärd, T., Ohlsson, U., Bernspång, L., et al., 2015. Assessment of the strengthening of an RC railway bridge with CFRP utilizing a full-scale failure test and finite-element analysis. *J. Struct. Eng.* 141 (D4014008), 1–11.
- Puurula, A.M., Enochsson, O., Sas, G., Blanksvärd, T., Ohlsson, U., Bernspång, L., et al., 2014. Loading to failure and 3D nonlinear FE modelling of a strengthened RC bridge. *Struct. Infrastruct. Eng.* 10, 1606–1619.
- Qian, Z., Lantsoght, E.O., Lukovic, M., 2022. A critical review on structural behavior of alkali-activated concrete beams. In: *Proceedings of the 14th fib International PhD Symposium in Civil Engineering*, fib. The International Federation for Structural Concrete, 273–280.
- Rafla, K., 1971. Empirical formula for calculation of shear capacity of reinforced concrete beams (in German). *Str. Brücke Tunn.* 23, 311–320.
- Rijkswaterstaat, 2002. Management- and maintenance plan Viaduct. Zijlweg of highway A59 (in Dutch). 36 pp.
- Rijkswaterstaat, 2013. Guidelines Assessment Bridges –assessment of structural safety of an existing bridge at reconstruction, usage and disapproval (in Dutch), RTD 1006:2013 1.1. Utrecht, the Netherlands.
- Rodriguez, A., Lantsoght, E.O.L., 2018. Verification of flexural stop criteria for proof load tests on concrete bridges based on beam experiments. IALCCE 2018, Ghent, Belgium.
- Sabatino, S., Frangopol, D.M., Dong, Y., 2015. Sustainability-informed maintenance optimization of highway bridges considering multi-attribute utility and risk attitude. *Eng. Struct.* 102, 310–321.
- Sanayei, M., Reiff, A.J., Brenner, B.R., Imbaro, G.R., 2016. Load rating of a fully instrumented bridge: comparison of LRFR approaches. *J. Perform. Constr. Facil.* 2016, 2.
- Schacht, G., Bolle, G., Curbach, M., Marx, S., 2016a. Experimental evaluation of the shear bearing safety (in German). *Beton- und Stahlbetonbau* 111, 343–354.
- Schacht, G., Bolle, G., Marx, S., 2016b. Load testing – international state of the art (in German). *Bautechnik* 93, 85–97.
- Schmidt, J.W., Hansen, S.G., Barbosa, R.A., Henriksen, A., 2014. Novel shear capacity testing of ASR damaged full scale concrete bridge. *Eng. Struct.* 79, 365–374.
- Siemes, T., Han, N., Visser, J., 2002. Unexpectedly low tensile strength in concrete structures. *Heron* 47, 111–124.
- Talley, K.G., 2009. Assessment and Strengthening of ASR and DEF Affected Concrete Bridge Columns (PhD thesis). The University of Texas at Austin.
- TNO Diana, 2012. Users Manual of DIANA, Rel. 9.4.4. Delft, The Netherlands.
- Thomas, R., Mann, J.E., Chill, Z.M., 2012. Bridge inspector's reference manual. FHWA NHI 12–049.
- Val, D.V., Stewart, M.G., 2019. Chapter 10: Determination of remaining service life of reinforced concrete bridge structures in corrosive environments after load testing. In: Lantsoght, E.O.L. (Ed.), *Load Testing of Bridges Volume 2: Proof Load Testing and the Future of Load Testing*. CRC Press, Boca Raton, FL.
- Vavruš, M., Bujňák, J., Koteš, P., 2019. Experimental verification of real behavior of bridge structures using proof-load tests. *Pollack Periodica* 14, 75–84.

- Velázquez, B.M., Yura, J.A., Frank, K.H., Kreger, M.E., Wood, S.L., 2000. Diagnostic load tests of a reinforced concrete pan-girder bridge. The University of Texas at Austin, Austin, TX, USA.
- Walraven, J., 1980. Aggregate Interlock: A Theoretical and Experimental Analysis (PhD thesis). Delft University of Technology.
- Walraven, J.C., 1981. Fundamental analysis of aggregate interlock. *J. Struct. Div.* 107, 2245–2270.
- Wang, Z., Yang, D.Y., Frangopol, D.M., Jin, W., 2019. Inclusion of environmental impacts in life-cycle cost analysis of bridge structures. *Sustain. Resilient Infrastruct.* 1–16.
- Wang, C., Zhang, H., 2020. A probabilistic framework to optimize the target proof load for existing bridges. *Innov. Infrastruct. Solut.* 5, 12.
- Witteveen + Bos, 2014. Material research bridges, case 31084913: 44G-113-01: viaduct Zijlweg (in Dutch). Deventer.
- Yang, Y., Den Uijl, J.A., Walraven, J., 2016. The Critical Shear Displacement theory: on the way to extending the scope of shear design and assessment for members without shear reinforcement. *Struct. Concr.* 17, 790–798.
- Yang, D.Y., Frangopol, D.M., Teng, J.-G., 2019. Probabilistic life-cycle optimization of durability-enhancing maintenance actions: application to FRP strengthening planning. *Eng. Struct.* 188, 340–349.
- Yang, Y., 2014. Shear Behaviour of Reinforced Concrete Members without Shear Reinforcement – A New Look at an Old Problem (PhD). Delft University of Technology.
- Yang, Y., Hordijk, D.A., 2015. Acoustic emission measurement and analysis on Zijlwegbrug. Delft. Delft University of Technology, The Netherlands.
- Yang, Y., Walraven, J., Den Uijl, J.A., 2017. Shear behavior of reinforced concrete beams without transverse reinforcement based on critical shear displacement. *J. Struct. Eng.* 143, 04016146–1-13.
- Yang, Y., Zárate Garnica, G., Lantsoght, E.O.L., Hordijk, D.A., 2018. Calibration of the shear stop criteria based on crack kinematics of reinforced concrete beams without shear reinforcement. fib conference 2018. Melbourne, Australia.
- Zarate Garnica, G.I., Lantsoght, E.O.L., 2019. Verification of Stop Criteria for Proof Load Tests. Delft University of Technology, Delft, the Netherlands.
- Zarate Garnica, G.I., Lantsoght, E.O.L., 2020. Preparation of Experiments on Reinforced Concrete Slabs for Determination of Stop Criteria Delft. Delft University of Technology, The Netherlands.
- Zarate Garnica, G.I., Lantsoght, E.O.L., 2021. Measurement Report of Reinforced Concrete Slabs. Delft University of Technology, Delft, the Netherlands.
- Zarate Garnica, G.I., Zhang, F., Yang, Y., Van Der Veen, C., Lantsoght, E.O.L., Naaktgeboren, M. et al., 2021. Monitoring structural responses during proof load testing of reinforced concrete bridges: a review. *Bridge Maintenance, Safety, Management, Life-Cycle Sustainability and Innovations*. In: Proc. 10th Int. Conf. Bridge Maintenance, Saf. Management, IABMAS 2020, 2339–2346.
- Zárate Garnica, G., 2018. Assessment of Crack Kinematics in Concrete Beams Using Digital Image Correlation. Delft University of Technology.
- Zhang, F., 2022. Acoustic Emission-Based Indicators of Shear Failure of Reinforced Concrete Structures Without Shear Reinforcement (PhD thesis). Delft University of Technology.

-
- Zhang, F., Zarate Garnica, G.I., Yang, Y., Lantsoght, E., Sliedrecht, H., 2020. Monitoring shear behavior of prestressed concrete bridge girders using acoustic emission and digital image correlation. *Sensors* 20, 5622.
- Zinke, T., Ummenhofer, T., Pfaffinger, M., Mensinger, M., 2012. The social dimension of bridge sustainability assessment – Impacts on users and the public. In: Biondini, F., Frangopol, D.M. (Eds.), *Proceedings of the Sixth International Conference on Bridge Maintenance, Safety and Management*. Taylor & Francis Group, Stresa, Lake Maggiore, Italy.